Displacement Centre of Gravity and Stability Arm in Longitudinal Tilt of a Floating Body with Circular Floats

Leopold Hrabovský * , Pavla Karbanová , Ladislav Kovář

Posted Date: 23 April 2026

doi: 10.20944/preprints202604.1700.v1

Keywords: floating belt conveyor; center of gravity of displacement; stability arm; displacement of floating body from equilibrium; buoyancy force; experimental setup

 doi:10.20944/preprints202604.1700.v1

Article

Displacement Centre of Gravity and Stability Arm in Longitudinal Tilt of a Floating Body with Circular Floats

Leopold Hrabovský *, Pavla Karbanová and Ladislav Kovář

Department of Machine and Industrial Design, Faculty of Mechanical Engineering, VSB–Technical University of Ostrava, 17. listopadu 2172/15, 708 00 Ostrava–Poruba, Czech Republic

* Correspondence: leopold.hrabovsky@vsb.cz

Abstract

Floating belt conveyor routes, consisting of serially arranged belt conveyors, the end parts of which are mechanically attached to floating bodies, are designed for the continuous transport of extracted granular materials from the water. The paper deals with the analytical determination of the position of the centre of gravity of the buoyancy force, the coordinates of which change depending on the longitudinal deflection of the floating body from the equilibrium state, which acts as a supporting element of individual conveyor belts. The analysis of the individual phases of deflection of the floating body, consisting of a pair of floats with a circular cross-section, shows that the complete submergence of one of the floats occurs at a higher value of the angle of inclination in the case when the floats are initially submerged under the surface to exactly half of their diameter. On the realized experimental device the buoyancy force was detected using strain gauges during the deflection of the floating body from the equilibrium position for three defined levels of immersion. The floating body of the experimental device consists of a pair of floats with a circular cross-section with a diameter of 80 mm. The output is a structured methodological procedure for determining the position of the centre of gravity of the displacement (centre of buoyancy) of a floating body when it deviates from the equilibrium position and a methodology for calculating the stability arm, which is a key parameter for assessing the buoyancy and stability of the body. On the basis of the laboratory measurements, the magnitude of the buoyancy force can be quantified as a function of the immersion depth of the floating body. It was found that the buoyancy force remains constant when the body deflects only when the immersion corresponds to half the diameter of a float with a circular cross-section. If the depth of the immersion is less than the radius of the float, the buoyancy force increases during deflection; on the contrary, if the immersion is greater than the radius of the float, the buoyancy force decreases.

Keywords: floating belt conveyor; center of gravity of displacement; stability arm; displacement of floating body from equilibrium; buoyancy force; experimental setup

1. Introduction

Floating belt conveyors [1] consist of two floating bodies [2], co called pontoons, of a rectangular [3] or circular [4] cross-section, see Figure 1 with several watertight chambers, equipped with overflows and a turning mechanism.

The main objective of this paper is to investigate the buoyancy of floating conveyors, considering the loss of stability it is essential to ensure their safe and reliable operation. Understanding the mechanisms that lead to loss of stability allows you to prevent accidents, minimise the risk of damage to equipment and the surrounding environment and optimise the design of conveyors. At the same time, it contributes to more efficient operation, extended equipment life and reduced economic losses associated with breakdowns or downtime.

 doi:10.20944/preprints202604.1700.v1

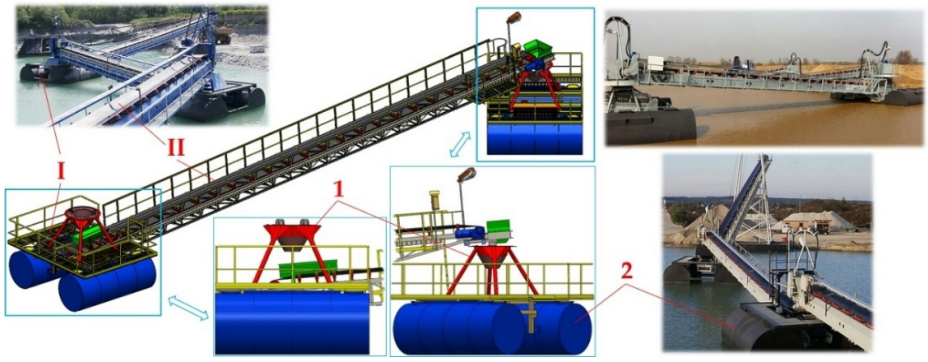

Figure 1. Floating belt conveyor. I – floating body, II – belt conveyor, 1 – turntable structure, 2 – float of a circular cross-section.

When designing the floating bodies of floating belt conveyors in the design of end floats, it is necessary to ensure the condition of unsinkability [5,6]. The unsinkability of the floating body of a floating conveyor belt is defined as the property of the floating body to retain its buoyancy [2,7–9] when one or more of its parts are flooded. In practice, unsinkability is ensured by dividing the partial floats by watertight transverse or even longitudinal watertight bulkheads (into so-called chambers). In order to ensure unsinkability [10–12], it is necessary to determine the optimum location and the minimum number of these chambers that is unavoidable, because flooding of the sub-chambers results in a change in the displacement and mean draught, a change in the longitudinal slope and a reduction in the metacentric stability height (the effect of the free surface in the flooded chambers).

For floating bodies, stability is important [13,14]. A body floats stably if, when deflected, a pair of forces acts on the body to bring it back to its original equilibrium position. A floating body can have essentially three positions [15,16] - stable (steady), unstable (wobbly) and indifferent (free).

For floating bodies, two points [1] are primarily important, which lie on a common vertical, the so-called axis of floating, during the equilibrium of the body. It is the centre of gravity "T" of the floating body, at which the gravitational force G_{FB} [N] of the body acts, and the centre of gravity "V" of the liquid body of volume V [m^3] displaced by the floating body, the point at which the buoyant force F_B[N] acts, see Figure 2.

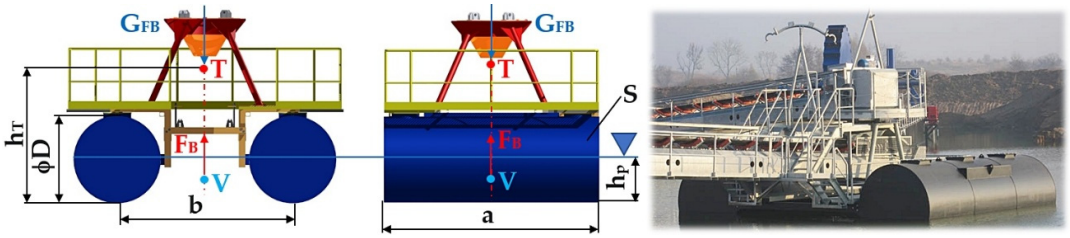

Figure 2. Floating body of a conveyor belt with circular floats.

For a homogeneous body [17], the point "T" is always above the point "V". In the centre of "T" gravity of a body, the downward force of gravity G_{FB} [N] tries to take the lowest possible position after the body is deflected, whereas the centre of gravity "V", in which the upward force of buoyancy F_B [N] acts, takes the highest possible position [1,2]. If we move the body out of this position by a small angle ϕ [deg] the shape of the liquid body changes, although its volume V [m^3] is preserved - the position of the centre of gravity "T" changes. When a floating body is deflected from a stable position, a pair of forces F_B [N], [N], G_{FB} [N], is generated which, by its moment of force, returns the deflected body to its equilibrium position. The stable position is easily judged by the point "M" [2], which is the intersection of the buoyancy force carrier and the deflected axis of float. The point "M" is called the metacenter [1] and the distance "TM" [2] is the metacentric height. For a stably floating

 doi:10.20944/preprints202604.1700.v1

body, the point "M" is above the point "T" and the metacentric height "TM" is defined to be positive. The greater the metacentric height "TM", the faster the deflected body returns to its equilibrium position.

If the metacentre "M" falls below the centre of gravity "T", the body is in an unstable position when floating, because when it is deflected from its equilibrium position by a small angle ϕ [deg], a pair of forces F_B [N], G_{FB} [N] begins to act on the boy by a knock-on moment of force which overturns it. The metacentric height "TM" is negative in this case.

In addition to the stable and labile position, the body may be in an indifferent position, where the metacentre "M" is at the centre of gravity "M". In the indifferent position during floating, there is probably a longer rotating cylinder with a horizontal axis or a sphere [1,2]. The metacentric height "TM" is zero.

Buoyancy [18] is defined as the ability of a body to float on a still liquid surface by the action of hydrostatic buoyancy [19]. Buoyancy is one of the basic properties of a floating body, characterized by the ability of the body to remain in an equilibrium state when immersed in a liquid. The buoyancy reserve is defined as the mass amount of load (which the floating body is capable of carrying) that will cause the total immersion of the floating body in the liquid [20].

Stability [21,22] falls inherently into a broader group of navigation properties of floating bodies. Stability of a floating body [23,24] is defined as the ability of a floating body to return to its equilibrium position after deflection if the external forces causing the deflection cease to act on it.

According to the direction of deflection of the floating body, two variants of stability are recognized, "transverse" stability [25–27] and "longitudinal" stability.

Depending on the amount of deflection of the floating body, we distinguish between "initial" stability and "high angle of heel" stability.

According to the time effect of external forces and the influence of inertia of masses, it is possible to define "static" stability (which is defined by the magnitude of the return moment when the body is deflected from the equilibrium position) and "dynamic" stability (which is determined by the magnitude of the work that the floating body is able to absorb when deflected from the equilibrium position).

The issue of stability of floating belt conveyors has not yet been fully investigated systematically, especially in the case of floating body designs using floats with circular cross-sections [28,29]. These specific designs of floating bodies can significantly affect the buoyancy distribution, the position of the centre of gravity and the overall stability behaviour of the system, but the available literature only marginally addresses this area. Insufficient knowledge of these influences poses a risk in the design and operation of the equipment, especially in terms of the possibility of loss of stability under variable operating conditions. Detailed research on this issue is therefore necessary to gain a deeper understanding of the behaviour of these systems, to refine design methods and to improve the safety and reliability of floating conveyors.

The current state of knowledge in the field of stability of floating bodies has been analysed on the basis of available literature. It was found that the vast majority of the publications searched focus mainly on the issue of buoyancy and stability of ships, while the specific area of floating conveyor belts remains virtually uncovered in professional sources. This disparity points to an existing gap in research and highlights the need for a focused study of the stability of these devices, whose design and operating conditions differ from conventional vessels in many respects.

The stability of a floating body of rectangular cross-section is addressed in [30,31]. For these types of floating bodies, the coordinates of the centre of gravity of the buoyancy force can be determined at different immersion depths and angles of deflection of the floating body from the equilibrium state using the relations of static moments of surfaces [1].

 doi:10.20944/preprints202604.1700.v1

2. Materials and Methods

The detailed description of the procedures and methods used in this section is intended to ensure the transparency of the research, to enable reproducibility of the results and to support their use in subsequent studies or practical applications.

The total gravity G_{FB} [N] acting on the floating body is assumed. The weight G_{FB} [N] acts at the centre of gravity "T", which is h_T [m] away from the bottom plane of the floating body, see Figure 2. In the equilibrium position ($\phi = 0$ deg), the horizontal axes of the floats of circular cross-section are parallel to the water surface. The buoyant force F_B [N] must be in balance with the gravity G_{FB} [N] (1).

$$F_B = \rho \cdot V_p \cdot g = \rho \cdot a \cdot S \cdot g = G_{FB}\ [N] \tag{1}$$

where ρ [kg − m^{-3}] is the density of water; V_p [m^3] is the total volume of the submerged parts of the two floats (2); S [m^2] is the submerged plan area of the floats; and [m] is the length of the floats.

$$S_o = \frac{\pi \cdot D^2}{4}[m^2]; V_p = 2 \cdot \frac{S}{2} \cdot a\ [m^3] \tag{2}$$

where D [m] is the diameter of the circular float.

2.1. Longitudinal Tilt of the Float Body When the Floats Are Submerged $h_p = \frac{D}{2}$ [m]

The 1st phase starts in the equilibrium position $\phi = \phi_0 = 0$ [deg], see Figure 2, and ends with the right cylindrical float dipping below the surface $\phi = \phi_1$ [deg] ($\phi_1 = \text{asin}\left(\frac{D}{b}\right)$ [deg]).

The area S [m^2] bounded by the circular faces of both floats (the left S_1 [m^2], according to Figure 3, and the right S_2 [m^2]) of its bottoms and surface, can be expressed according to relation (3).

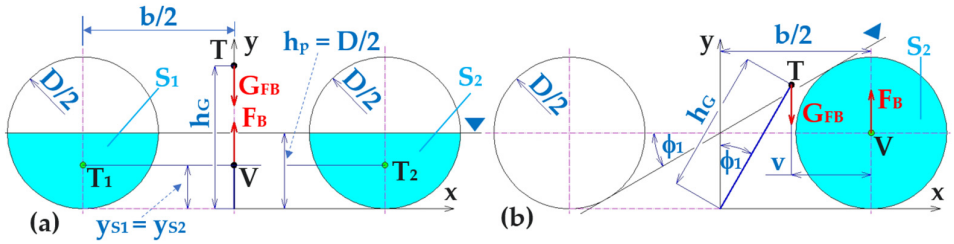

Figure 3. Floating body **(a)** in equilibrium state $\phi = 0$ deg, **(b)** when deflected by an angle of $\phi = \phi_1$ [deg].

$$S = S_1 + S_2\ [m^2] \tag{3}$$

where S_1 [m^2] is the sumberged area of the left float; S_2 [m^2] is the submerged area of the right float.

According to Figure 4, the relation (4) applies to the length x_1 [m] and the height of the circular segment v [m].

$$\sin(\phi) = \frac{2 \cdot x_1}{b} \Rightarrow x_1 = \sin(\phi) \cdot \frac{b}{2}\ [m];\ v = \frac{D}{2} - x_1\ [m] \tag{4}$$

 doi:10.20944/preprints202604.1700.v1

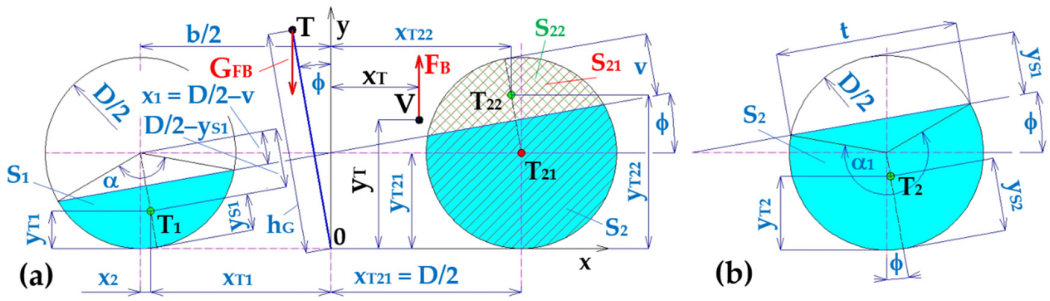

Figure 4. (a) the area of immersion of the left $S_1\,[m^2]$ float and right float $S_2\,[m^2]$ at deflection ϕ [deg] of the floating body, **(b)** coordinates $y_{T2}[m]$ of the centre of gravity T_2 of the right float.

The central angle α [deg] of the submerged area (circular segment) $S_1\,[m^2]$ of the left float of the floating body can be expressed according to (5).

$$\alpha = 2 \cdot \operatorname{asin}\left(\frac{x_1}{D}\right)\ [\text{deg}] \tag{5}$$

The length of the chord $t\,[m]$, the angle $\alpha\,[\text{deg}]$ (see Figure 4a) and the angle $\alpha_1[\text{deg}]$ (see Figure 4b) are given by relation (6).

$$t = 2 \cdot \sqrt{v \cdot (D - v)}\ [m];\ \alpha = 2 \cdot \operatorname{asin}\left(\frac{t}{D}\right)[\text{deg}];\ \alpha_1 = 2 \cdot \left[\pi - \operatorname{asin}\left(\frac{t}{D}\right)\right][\text{deg}] \tag{6}$$

Distance of the centre of gravity $y_{S1}[m]$ of the submerged area $S_1[m^2]$ of the left float, see Figure 4a, and the distance of the centre of gravity $y_{S2}\,[m]$ of the immersed area $S_2\,[m^2]$ of the right float, see Figure 4b, can be expressed according to the relation (7).

$$\begin{aligned} y_{S1} &= \frac{2 \cdot \left(\frac{D}{2}\right)^3 \cdot \left[\frac{\alpha}{4} - \frac{\sin(\alpha)}{4} - \frac{\sin\left(\frac{\alpha}{2}\right)^3}{3}\right]}{\left(\frac{D}{2}\right)^2 \cdot \left[\frac{\alpha}{2} - \frac{\sin(\alpha)}{2}\right]}\ [m]; \\ y_{S2} &= \frac{2 \cdot \left(\frac{D}{2}\right)^3 \cdot \left[\frac{\alpha_1}{4} - \frac{\sin(\alpha_1)}{4} - \frac{\sin\left(\frac{\alpha_1}{2}\right)^3}{3}\right]}{\left(\frac{D}{2}\right)^2 \cdot \left[\frac{\alpha_1}{2} - \frac{\sin(\alpha_1)}{2}\right]}\ [m] \end{aligned} \tag{7}$$

Area $S_1\,[m^2]$ of the submerged part of the left float and the area of $S_2\,[m^2]$ of the submerged part of the right float can be analytically determined according to (8).

$$S_1 = \frac{1}{2} \cdot \left(\frac{D}{2}\right)^2 \cdot [\alpha - \sin(\alpha)]\ [m^2];\ S_2 = \left(\frac{D}{2}\right)^2 \cdot \left[\pi - \frac{\alpha - \sin(\alpha)}{2}\right][m^2] \tag{8}$$

The coordinates of the centres of gravity of the sub-plots $S_1[m^2]$, $S_{21}[m^2]$ and $S_{22}[m^2]$ are given in relations (9) and (10).

$$x_{T1} = \frac{-b}{2} + \left(\frac{D}{2} - y_{S1}\right) \cdot \sin(\phi)\ [m];\ x_{T21} = \frac{b}{2}\ [m];\ x_{T22} = \frac{b}{2} - \left(\frac{D}{2} - y_{S1}\right) \cdot \sin(\phi)\ [m] \tag{9}$$

$$y_{T1} = \frac{D}{2} - \left(\frac{D}{2} - y_{S1}\right) \cdot \cos(\phi)\ [m];\ y_{T21} = \frac{D}{2}\ [m];\ y_{T22} = \frac{D}{2} + \left(\frac{D}{2} - y_{S1}\right) \cdot \cos(\phi)\ [m] \tag{10}$$

The coordinates of the centre of gravity of the displacement $x_T[m]$, $y_T\,[m]$ are given by the relation (11).

$$x_T = \frac{S_1 \cdot x_{T1} + S \cdot x_{T21} - S_1 \cdot x_{T22}}{S}\ [m];\ y_T = \frac{S_1 \cdot y_{T1} + S \cdot y_{T21} - S_1 \cdot y_{T22}}{S}\ [m] \tag{11}$$

 doi:10.20944/preprints202604.1700.v1

The stability arm s_a [m], see Figure 5, is given by relation (12).

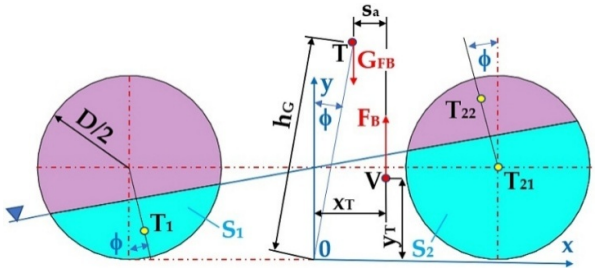

Figure 5. Arm stability s_a [m] of a floating body deflected from equilibrium by an angle of ϕ [deg].

$$s_a = x_T \cdot \cos(\phi) + y_T \cdot \sin(\phi) - h_G \cdot \sin(\phi) \text{ [m]} \quad (12)$$

The coordinates of the centre of gravity $\{x_T, y_T\}$ [m, m] of the buoyant force F_B [N] of the floating body during the first phase of deflection $0 \le \phi \le \phi_1$ [deg], analytically calculated according to (11) at the float immersion depth (in the equilibrium state $\phi = 0$ deg) of the floating body h_p = 795 mm, are given in Table 1.

Table 1. Coordinates of the centre of gravity $\{x_T, y_T\}$ [m, m] of the buoyant force F_B [N] of the floating body during phase 1 of the deflection $0 \le \phi \le \phi_1$ at the immersion depth of h_p = 795 mm.

b = 3.18 m; D = 1.59 m; h_G = 1.6 m; h_p = 0.795 m								
ϕ	[deg]	0	5	10	15	20	25	30 = ϕ_1
x_T		0	379.17	737	1053.74	1312.36	1498.29	1590
$x_T \cdot \cos(\phi)$		0	377.73	725.80	1017.83	1233.22	1357.91	1376.98
y_T	10^{-3}	457.59	474.08	520.98	590.87	671.94	748.33	795
$y_T \cdot \sin(\phi)$	$\cdot$ m	0	41.32	90.47	152.93	229.82	316.26	397.50
$h_G \cdot \sin(\phi)$		0	139.45	277.84	414.11	547.23	676.19	800
s_a[1]		0	279.60	538.43	756.65	915.80	997.98	974.48
S_1	10^{-4}	9927.83	7735.65	5627.75	3689.87	2013.25	708.50	974.48
S_2	$\cdot$ m^2	9927.83	12120.00	14227.91	16165.78	17842.40	19147.15	19855.65
S					19855.65			
V_1	10^{-6}	3971130.19	3094260.27	2251098.18	1475948.36	805300.66	283401.91	0
V_2	$\cdot$ m^3	3971130.19	4848000.11	5691162.21	6466312.03	7136959.72	7658858.48	7942260.39
V					7942260.39			
b = 3.18 m; D = 1.59 m; h_G = 2.0 m								
$h_G \cdot \sin(\phi)$	10^{-3}	0	174.31	347.30	517.64	684.04	845.24	1000
s_a[1]	$\cdot$ m	0	244.73	468.97	653.12	778.99	828.93	774.48
b = 3.18 m; D = 1.59 m; h_G = 2.5 m								

 doi:10.20944/preprints202604.1700.v1

$h_G \cdot \sin(\phi)$	$10^{-3} \cdot m$	0	217.89	434.12	647.05	855.05	1056.55	1250
s_a[1]		0	201.16	382.15	523.72	607.98	617.62	524.48

[1] see Figure 6.

Figure 6 presents the size of the stability arm s_{and} [m] (12) when the floating turntable is deflected out of equilibrium, with the floats' immersion depth (in the steady state $\phi = 0$ deg) of the floating body $h_p = 795$ mm.

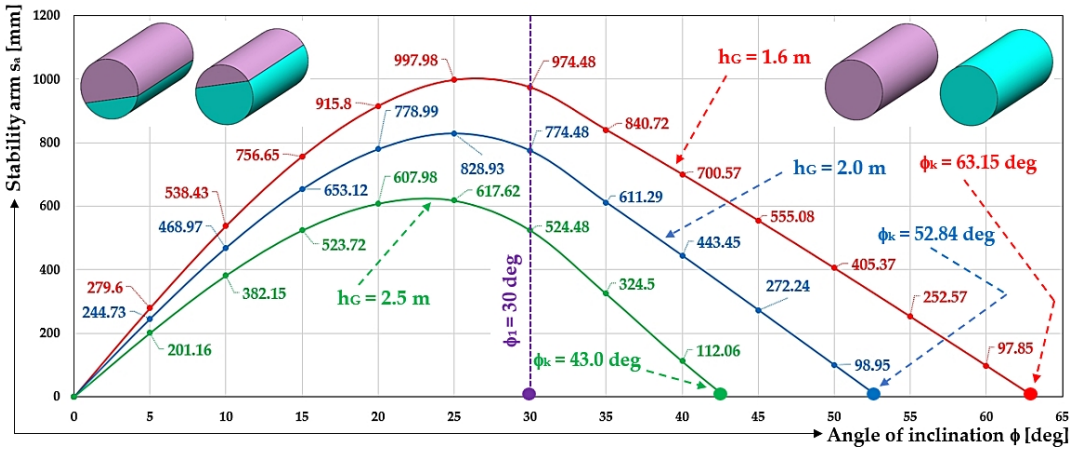

Figure 6. Stability arm size s_{and}[m] at deflection ϕ [deg] of the floating turn from equilibrium, at h_p = 795 mm.

2nd phase begins by submerging the right cylindrical float below the surface $\phi = \phi_1 = 30$ deg (13) and ends with the loss of buoyancy of the floating body ϕ_k [deg] (13).

$$\phi_1 = \operatorname{asin}\left(\frac{D}{b}\right) \text{ [deg]; } \phi_k = \operatorname{atan}\left(\frac{b}{2 \cdot h_G - D}\right) \text{ [deg]} \quad (13)$$

The coordinates of the centre of gravity $\{x_T, y_T\}$ [m, m] of the buoyancy force F_B [N] of the floating body during the second phase of the deflection $\phi_1 \le \phi \le \phi_k$, at the float immersion depth (in the equilibrium state $\phi = 0$ deg) of the floating body $h_p = 795$ mm, are given in Table 2.

Table 2. Coordinates of the centre of gravity $\{x_T, y_T\}$ [m, m] of the buoyant force F_B [N] of the floating body during phase 2 of the deflection $\phi_1 \le \phi \le \phi_k$ [deg] at the immersion depth of $h_p = 795$ mm.

b = 3.18 m; D = 1.59 m; h_G = 1.6 m; h_p = 0.795 m									
ϕ	[deg]	35	40	45	50	55	60	65	63.15 = ϕ_k
x_T		1590							
$x_T \cdot \cos(\phi)$		1302.45	1218.01	1124.30	1022.03	911.99	795.00	671.96	718.13
y_T		795							
$y_T \cdot \sin(\phi)$	$10^{-3} \cdot m$	455.99	511.15	562.15	609.01	651.23	688.49	720.51	709.29
$h_G \cdot \sin(\phi)$		917.72	1028.46	1131.37	1225.67	1310.64	1385.64	1450.09	1427.51
s_a[1]		840.72	700.57	555.08	405.37	252.57	97.85	–57.61	0
S_2		19855.65							

Preprints.org (www.preprints.org) | NOT PEER-REVIEWED | Posted: 23 April 2026 doi:10.20944/preprints202604.1700.v1

V	$10^{-6}\cdot m^3$	7942260.39					
		b = 3.18 m; D = 1.59 m; h_G = 2.0 m					
ϕ	[deg]	35	40	45	50	55	52.84 = ϕ_k
$h_G \cdot \sin(\phi)$	$10^{-3}\cdot m$	1147.15	1285.58	1414.21	1532.09	1683.30	1593.9
s_a^2		611.29	443.45	272.24	98.95	–75.09	0
		b = 3.18 m; D = 1.59 m; h_G = 2.5 m					
ϕ	[deg]	35	40	45	43.00 = ϕ_k		
$h_G \cdot \sin(\phi)$	$10^{-3}\cdot m$	1433.94	1606.97	1767.77	1705.00		
s_a^3		324.50	112.06	–81.32	0		

$s_a = 0$ m for ϕ_k [deg] = [1] 63.15; [2] 52.84; [3] 43.00, see Figure 6.

Figure 7 presents the deflection of the floating body during phase 2. The left float of the circular cross-section S_1 [m^2] is completely above the water surface and the right float of the floating body of the cross-section $S_2 = S$ [m^2] (2) is completely submerged below the water surface.

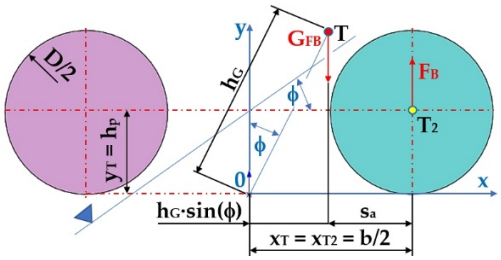

Figure 7. 2d phase of floating body deflection from the equilibrium state $\phi_1 \le \phi \le \phi_k$ [deg].

2.2. Longitudinal Tilt of the Float Body When the Floats Are Submerged $h_p < \frac{D}{2}$ [m]

The total gravity G_{FB} [N] acting on the floating body is assumed. The weight G_{FB} [N] acts at the centre of gravity T, which is h_T [m] away from the bottom plane of the floating body, see Figure 2. In the equilibrium position ($\phi = 0$ deg), the horizontal axes of the floats of circular cross-section are parallel to the water surface. The buoyant force F_B [N] must be in balance with the gravity G_{FB} [N] (1).

Displacement of the floating body from the equilibrium state during phase 1, when the floats $h_p < \frac{D}{2}$ [m] and $h_p > \frac{D}{2}$ [m] are submerged, is stated in Figure 8.

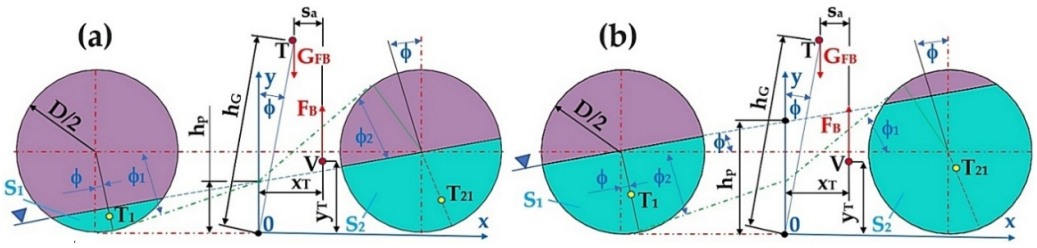

Figure 8. Displacement of the floating body from the equilibrium state during phase 1, when the floats **(a)** $h_p < \frac{D}{2}$ [m], **(b)** $h_p > \frac{D}{2}$ [m] are submerged.

 doi:10.20944/preprints202604.1700.v1

The 1st phase starts in the equilibrium position $\phi = \phi_0 = 0$ deg, see Figure 2, and ends with the left float of circular cross section emerging above the water surface $\phi = \phi_1 = 18.94$ deg (16), see Figure 9a.

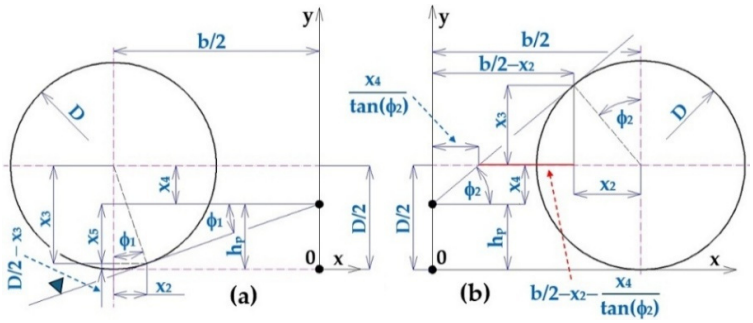

Figure 9. Total immersion of the **(a)** left float $\phi = \phi_1$[deg], **(b)** right float $\phi = \phi_2$[deg] of the floating body at $h_p < \frac{D}{2}$ [m].

$$x_2 = \frac{D}{2} \cdot \sin(\phi_1)\ [m];\ x_3 = \frac{D}{2} \cdot \cos(\phi_1)\ [m]; x_4 = \frac{D}{2} - h_p\ [m] \tag{14}$$

$$x_5 = \frac{D}{2} - \left(\frac{D}{2} - x_3\right) - x_4 = \frac{D}{2} \cdot [\cos(\phi_1) - 1] + h_p\ [m] \tag{15}$$

$$\tan(\phi_1) = \frac{x_5}{\frac{b}{2} - x_2} \Rightarrow \phi_1 = \operatorname{atan}\left\{\frac{\frac{D}{2} \cdot [\cos(\phi_1) - 1] + h_p}{\frac{b}{2} - \frac{D}{2} \cdot \sin(\phi_1)}\right\}\ [deg] \tag{16}$$

The magnitude of the angle $\phi_1 = 18.94$ deg can be determined in the Mathcad programming environment (version 14.0.0.163) [32] by the "Given–Find" instruction, or analytically from the quadratic Equation (17) derived from relation (16), see (18).

$$A_1 \cdot [\cos(\phi_1)]^2 + B_1 \cdot \cos(\phi_1) + C_1 = 0, \tag{17}$$

where $A_1 = \left(\frac{b}{2}\right)^2 + \left(h_p - \frac{D}{2}\right)^2\ [m^2]; B_1 = D \cdot \left(h_p - \frac{D}{2}\right)\ [m^2];\ C_1 = \frac{D^2 - b^2}{4}\ [m^2]$.

$$\phi_1 = \operatorname{acos}\left(\frac{-B_1 + \sqrt{B_1^2 - 4 \cdot A_1 \cdot C_1}}{2 \cdot A_1}\right)[deg] \tag{18}$$

The coordinates of the centre of gravity $\{x_T, y_T\}\,[m, m]$ of the buoyant force $F_B\,[N]$ of the floating body during the first phase of the deflection $0 \le \phi \le \phi_1$ [deg], where ϕ_1 [deg] can be determined according to (16), (18), at the float immersion depth (in the equilibrium state $\phi = 0$ deg) of the floating body $h_p = 500$ mm, are given in Table 3.

Table 3. Coordinates of the centre of gravity $\{x_T, y_T\}\,[m, m]$ of the buoyant force $F_B\,[N]$ of the floating body during phase 1 of the deflection $0 \le \phi \le \phi_1$ at the immersion depth of $h_p = 500$ mm.

b = 3.18 m; D = 1.59 m; h_G = 1.6 m; h_p = 0.5 m							
ϕ	[deg]	0	5	10	15	20	18.94 = ϕ_1
x_T		0	635.32	1171.33	1534.46	1658.01	1659.32
$x_T \cdot \cos(\phi)$	10^{-3} · m	0	632.90	1153.53	1482.17	1558.02	1569.48
y_T		293.39	324.57	407.68	515.62	608.15	593.00

 doi:10.20944/preprints202604.1700.v1

$y_T \cdot \sin(\phi)$		0	28.29	70.79	133.45	208.00	192.47
$h_G \cdot \sin(\phi)$		0	139.45	277.84	414.11	547.23	519.32
s_a [1]		0	521.74	946.49	1201.52	1218.79	1242.63
S_1	$10^{-4} \cdot m^2$	5347.31	3407.81	1753.74	510.21	0	0
S_2		5347.31	7474.35	9698.60	11931.82	14085.96	13640.31
S		10694.61	10882.17	11452.34	12442.02		
V_1	$10^{-6} \cdot m^3$	2138922.78	1363125.54	701497.43	204081.82	0	0
V_2		2138922.78	2989741.69	3879438.75	4772727.82	5634383.67	5456122.06
V		4277845.56	4352867.23	4580936.18	4976809.64	5634383.67	5456122.06
		$b = 3.18$ m; $D = 1.59$ m; $h_G = 2.0$ m; $h_p = 0.5$ m					
ϕ	[deg]	0	5	10	15	20	18.94 = ϕ_1 [2]
$h_G \cdot \sin(\phi)$	$10^{-3} \cdot m$	0	174.31	347.3	517.64	684.04	649.16
s_a [1]		0	486.88	877.03	1097.99	1081.98	1112.80
		$b = 3.18$ m; $D = 1.59$ m; $h_G = 2.5$ m; $h_p = 0.5$ m					
ϕ	[deg]	0	5	10	15	20	18.94 = ϕ_1 [2]
$h_G \cdot \sin(\phi)$	$10^{-3} \cdot m$	0	217.89	434.12	647.05	855.05	811.44
s_a [1]		0	443.30	790.21	968.58	910.97	950.51

[1] see Figure 10; [2] see Table 3.

Figure 10 presents the size of the stability arm s_a [m] (12) when the floating turntable is deflected out of equilibrium, with the floats' immersion depth (in the steady state $\phi = 0$ deg) of the floating body $h_p = 500$ mm.

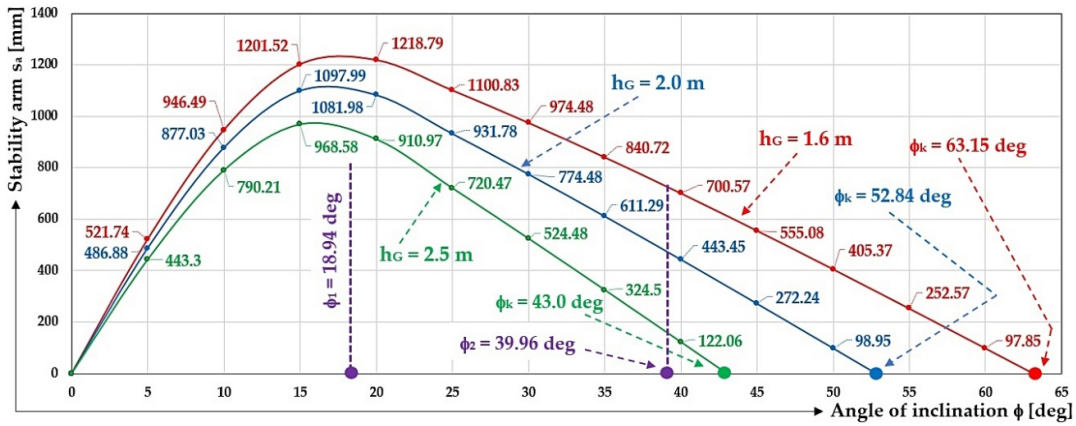

Figure 10. Stability arm size s_a [m] at deflection ϕ [deg] of the floating turn from equilibrium, at $h_p = 500$ mm.

The 2nd phase begins with by bringing the left cylindrical float above the surface $\phi_1 = 18.94$ deg (see Figure 10) and ends with after the right cylindrical float below the water surface $\phi = \phi_2$ [deg]

 doi:10.20944/preprints202604.1700.v1

(19) ($\phi_2 = 39.96$ deg), see Figure 9b, assuming that the length distances x_2 [m], x_3 [m] a x_4 [m] are determined by (14).

$$\tan(\phi_2) = \frac{x_3}{\frac{b}{2} - \frac{x_4}{\tan(\phi_2)} - x_2} \Rightarrow \phi_2 = \operatorname{atan}\left\{\frac{\frac{D}{2}\cdot\cos(\phi_2)}{\frac{b}{2} - \frac{\frac{D}{2} - h_p}{\tan(\phi_2)} - \frac{D}{2}\cdot\sin(\phi_2)}\right\}\ [\text{deg}] \tag{19}$$

The magnitude of the angle $\phi_2 = 39.96$ deg was solved in the Mathcad programming environment (version 14.0.0.163) [32] with the instruction "Given–Find", or analytically from the quadratic Equation (20) derived from relation (19), see (21).

$$A_2 \cdot [\cos(\phi_2)]^2 + B_2 \cdot \cos(\phi_2) + C_2 = 0, \tag{20}$$

where $A_2 \cdot [\cos(\phi_2)]^2 + B_2 \cdot \cos(\phi_2) + C_2 = 0$.

$$\phi_2 = \operatorname{acos}\left(\frac{-B_2 + \sqrt{B_2^2 - 4\cdot A_2 \cdot C_1}}{2 \cdot A_2}\right)[\text{deg}] \tag{21}$$

The coordinates of the centre of gravity $\{x_T, y_T\}$ [m, m] of the buoyancy force F_B [N] of the floating body during the second phase of the deflection $\phi_1 \le \phi \le \phi_2$ [deg], the magnitude of the angle ϕ_2 [deg] see (19), (21), at the float immersion depth (in the equilibrium state $\phi = 0$ deg) of the floating body $h_p = 500$ mm, are given in Table 4.

Table 4. Coordinates of the centre of gravity $\{x_T, y_T\}$ [m, m] of the buoyancy force F_B [N] of the floating body during the 2nd phase of deflection $\phi_1 \le \phi \le \phi_2$ [deg] at the immersion depth $h_p = 500$ mm.

b = 3.18 m; D = 1.59 m; h_G = 1.6 m; h_p = 0.5 m						
ϕ	[deg]	25	30	35	40	39.96 = ϕ_2 [1]
x_T	$10^{-3}\cdot$ m	1646.19	1627.30	1605.60	1590	1590
$x_T \cdot \cos(\phi)$		1491.95	1409.28	1315.23	1218.01	1218.72
y_T		674.51	730.40	772.72	795	795
$y_T \cdot \sin(\phi)$		285.06	365.20	443.21	511.02	510.59
$h_G \cdot \sin(\phi)$		676.19	800.00	917.72	1028.46	1027.60
s_a^2		1100.83	974.48	840.72	700.57	701.71
S_1	$10^{-3}\cdot$ m^2			0		
S_2		16071.35	17792.48	19133.29	19855.65	19855.65
V_1	$10^{-6}\cdot$ m^3			0		
$V_2 = V$		6428540.83	7116990.81	7653314.24	7942260.39	7942260.39
b = 3.18 m; D = 1.59 m; h_G = 2.0 m; h_p = 0.5 m						
ϕ	[deg]	25	30	35	40	39.96 = ϕ_2 [1]
$h_G \cdot \sin(\phi)$	$10^{-3}\cdot$ m	845.24	1000	1147.15	1285.58	1284.51
s_a^2		931.78	774.48	611.29	443.45	444.81
b = 3.18 m; D = 1.59 m; h_G = 2.5 m; h_p = 0.5 m						
ϕ	[deg]	25	30	35	40	39.96 = ϕ_2 [1]
$h_G \cdot \sin(\phi)$	$10^{-3}\cdot$ m	1056.55	1250.00	1433.94	1606.97	
s_a^2		720.47	524.48	324.50	122.06	123.68

[1] see (18); [2] see Figure 10.

 doi:10.20944/preprints202604.1700.v1

The 3rd phase begins in the right cylindrical float below the water surface $\phi = \phi_2 = 39.96$ deg (19), (21), see Figure 12b, and ends with the loss of buoyancy of the floating body ϕ_k [deg], see Table 7.

The coordinates of the centre of gravity $\{x_T, y_T\}$ [m, m] of the buoyancy force F_B [N] of the floating body during the 3rd phase of the deflection $\phi_2 \le \phi \le \phi_k$ [deg], at the float immersion depth (in the equilibrium state $\phi = 0$ deg) of the floating body $h_p = 500$ mm, are given in Table 5.

Table 5. Coordinates of the centre of gravity $\{x_T, y_T\}$ [m, m] of the buoyancy force F_B [N] of the floating body during the 3rd phase.

b = 3.18 m; D = 1.59 m; h_G = 1.6 m; h_p = 0.5 m							
ϕ	[deg]	45	50	55	60	65	63.15 = ϕ_k [1]
x_T					1590		
$x_T \cdot \cos(\phi)$		1124.30	1022.03	911.99	795.00	671.96	718.13
y_T					795		
$y_T \cdot \sin(\phi)$	$10^{-3} \cdot$ m	562.15	609.01	651.23	688.49	720.51	709.29
$h_G \cdot \sin(\phi)$		1131.37	1225.67	1310.64	1385.64	1450.09	1427.51
s_a [1]		555.08	405.37	252.57	97.85	–57.61	0
S_1	$10^{-3} \cdot m^2$				0		
S_2					19855.65		
V_1	$10^{-6} \cdot m^3$				0		
$V_2 = V$					7942260.39		
b = 3.18 m, D = 1.59 m, h_G = 2.0 m, h_p = 0.5 m							
ϕ	[deg]	45	50	55	52.84 = ϕ_k [1]		
$h_G \cdot \sin(\phi)$	$10^{-3} \cdot$ m	1414.21	1532.09	1638.30	1593.90		
s_a [1]		272.24	98.95	–75.09	0		
b = 3.18 m; D = 1.59 m; h_G = 2.5 m; h_p = 0.5 m							
ϕ	[deg]	45	43.00 = ϕ_k [1]				
$h_G \cdot \sin(\phi)$	$10^{-3} \cdot$ m	1767.77	1705.00				
s_a [1]		–81.32	0				

[1] see Figure 10.

2.3. Longitudinal Tilt of the Float Body When the Floats Are Submerged $h_p > \frac{D}{2}$ [m]

The 1st phase starts in the equilibrium position $\phi = \phi_0 = 0$ deg, see Figure 2, and ends with the right float of the float body submerged below the water surface $\phi = \phi_1 = 18.94$ deg (16), (18), see Figure 16a and Table 11.

$$x_6 = h_p - \frac{D}{2} \text{ [m]};$$

$$x_7 = \frac{D}{2} - \left(\frac{D}{2} - x_3\right) - x_6 = \frac{D}{2} \cdot [1 + \cos(\phi_1)] - h_p \text{ [m]}; \tag{22}$$

$$x_8 = \frac{x_6}{\tan(\phi_2)} \text{ [m]}$$

where the distance x_3[m] is stated in (14).

$$\tan(\phi_1) = \frac{x_7}{\frac{b}{2} - x_2} \Rightarrow \phi_1 = \operatorname{atan}\left\{\frac{\frac{D}{2} \cdot [1 + \cos(\phi_1)] - h_p}{\frac{b}{2} - \frac{D}{2} \cdot \sin(\phi_1)}\right\} \text{ [deg]} \tag{23}$$

 doi:10.20944/preprints202604.1700.v1

The magnitude of the angle $\phi_1 = 18.94$ deg (23) was solved in the Mathcad programming environment (version 14.0.0.163) [32] by the "Given–Find" instruction, or analytically from the quadratic Equation (24) derived from relation (23), see (25).

$$A_3 \cdot [\cos(\phi_1)]^2 + B_3 \cdot \cos(\phi_1) + C_3 = 0 \tag{24}$$

where $A_3 = A_2\ [m^2]; B_3 = B_2\ [m^2]; C_3 = C_1\ [m^2]$.

$$\phi_1 = \operatorname{acos}\left(\frac{-B_2 + \sqrt{B_2^2 - 4 \cdot A_2 \cdot C_1}}{2 \cdot A_2}\right)[\text{deg}] \tag{25}$$

The coordinates of the centre of gravity $\{x_T, y_T\}\ [m, m]$ of the buoyant $F_B\ [N]$ force during the first phase of the deflection $0 \le \phi \le \phi_1$ [deg], analytically calculated according to (18) at the float immersion depth (in the equilibrium $\phi = 0$ deg) of the floating $h_p = 1090$ mm body, are given in Table 6.

Table 6. Coordinates of the centre of gravity $\{x_T, y_T\}\ [m, m]$ of the buoyancy force $F_B\ [N]$ of the floating body during phase 1 of the deflection $0 \le \phi \le \phi_1$ at immersion depth $h_p = 1090$ mm.

b = 3.18 m; D = 1.59 m; h_G = 1.6 m; h_p = 1.09 m							
ϕ	[deg]	0	5	10	15	20	18.94 = ϕ_1^2
x_T		0	239.82	474.70	700.12	911.39	868.56
$x_T \cdot \cos(\phi)$		0	238.91	467.49	676.26	856.43	821.54
y_T	10^{-3}	610.12	617.42	638.03	667.53	692.29	689.34
$y_T \cdot \sin(\phi)$	$\cdot$ m	0	53.81	110.79	172.77	236.78	223.74
$h_G \cdot \sin(\phi)$		0	139.45	277.84	414.11	547.23	519.32
s_a^1		0	153.27	300.44	434.92	545.97	525.96
S_1	10^{-3}	14508.34	12381.30	10157.05	7923.83	5769.69	6211.11
S_2	$\cdot$ m^2	14508.34	16447.84	18101.91	19345.45	19855.65	19855.65
V_1		5803337.61	4952518.69	4062821.64	3169532.57	2307876.72	2484443.55
V_2	10^{-6}	5803337.61	6579134.85	7240762.95	7738178.57	7942260.39	7942260.39
V	$\cdot$ m^3	11606675.22	11531653.55	11303584.59	10907711.14	10250137.11	10426703.94
b = 3.18 m; D = 1.59 m; h_G = 2.0 m; h_p = 1.09 m							
ϕ	[deg]	0	5	10	15	20	18.94 = ϕ_1^2
$h_G \cdot \sin(\phi)$	10^{-3} $\cdot$ m	0	174.31	347.3	517.64	684.04	649.16
s_a^1		0	118.41	230.98	331.40	409.16	396.12
b = 3.18 m; D = 1.59 m; h_G = 2.5 m; h_p = 1.09 m							
ϕ	[deg]	0	5	10	15	20	18.94 = ϕ_1^2
$h_G \cdot \sin(\phi)$	10^{-3} $\cdot$ m	0	217.89	434.12	647.05	855.05	811.44
s_a^1		0	74.83	144.16	201.99	238.15	233.84

 doi:10.20944/preprints202604.1700.v1

[1] see Figure 12, [2] see Figure 11a.

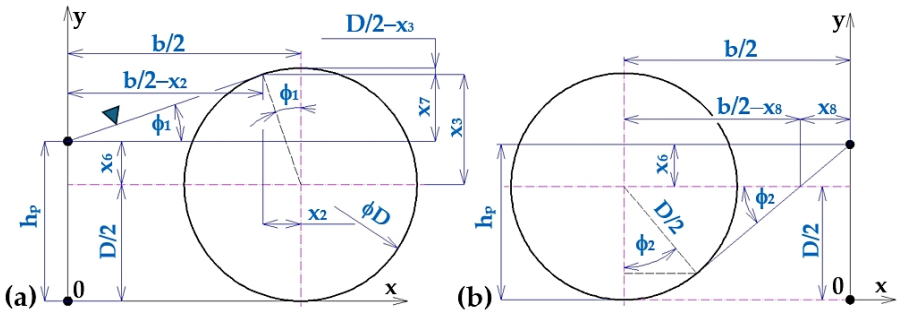

Figure 11. Total draft of the **(a)** left float $\phi = \phi_1$[deg], **(b)** right float $\phi = \phi_2$ [deg] of the floating body at $h_p > \frac{D}{2}$ [m].

Figure 12 presents the size of the stability arm s_a [m] (12) when the floating turntable is deflected from its equilibrium state, with the floats' immersion depth (in the steady state $\phi = 0$ deg) of the floating body $h_p = 1090$ mm.

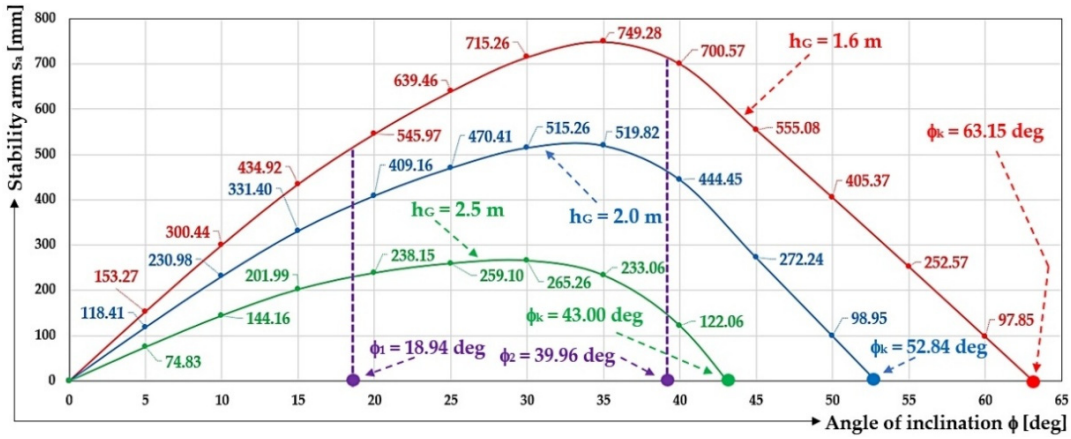

Figure 12. Stability arm size s_a [m] at deflection ϕ [deg] of the floating turn from equilibrium, at h_p = 1090 mm.

The 2nd phase begins by plunging the right float of the float body below the water surface $\phi_1 = 18.94$ deg (23), see Figure 11a and ends with the right float of the float body rising above the water surface $\phi_2 = 39.96$ deg (26), () see Figure 11b and Table 7.

$$\sin(\phi_2) = \frac{\frac{D}{2}}{\frac{b}{2} - x_8} \Rightarrow \phi_2 = \operatorname{asin}\left(\frac{\frac{D}{2}}{\frac{b}{2} - \frac{h_p - \frac{D}{2}}{\tan(\phi_2)}}\right) \text{[deg]} \tag{26}$$

where the distance x_8[m] is stated in (22).

The magnitude of the angle $\phi_2 = 39.96$ deg(26) was solved in the Mathcad programming environment (version 14.0.0.163) [32] by the "Given–Find" instruction, or analytically from the quadratic Equation (27) derived from relation (26), see (28).

$$A_4 \cdot [\cos(\phi_2)]^2 + B_4 \cdot \cos(\phi_2) + C_4 = 0 \tag{27}$$

$$\text{where } A_4 = A_1\ [\text{m}^2]; B_4 = B_1\ [\text{m}^2]; C_4 = C_1\ [\text{m}^2].$$

 doi:10.20944/preprints202604.1700.v1

$$\phi_2 = \operatorname{acos}\left(\frac{-B_1 + \sqrt{B_1^2 - 4 \cdot A_1 \cdot C_1}}{2 \cdot A_1}\right) [\text{deg}] \tag{28}$$

The coordinates of the centre of gravity $\{x_T, y_T\}$ [m, m] of the buoyancy force F_B [N] of the floating body during the second phase of the deflection $\phi_1 \le \phi \le \phi_2$ [deg], at the float immersion depth (in the equilibrium state $\phi = 0$ deg) of the floating body $h_p = 1090$ mm, are given in Table 7.

Table 7. Coordinates of the centre of gravity $\{x_T, y_T\}$ [m, m] of the buoyancy force F_B [N] of the floating body during the 2nd phase of deflection $\phi_1 \le \phi \le \phi_2$ [deg] at immersion depth $h_p = 1090$ mm.

b = 3.18 m; D = 1.59 m; h_G = 1.6 m; h_p = 1.09 m						
ϕ	[deg]	25	30	35	40	39.96 = ϕ_2 [1]
x_T		1119.14	1320.95	1492.88	1590	1590
$x_T \cdot \cos(\phi)$		1014.29	1143.98	1222.90	1218.01	1218.72
y_T	$10^{-3} \cdot$ m	713.09	742.56	774.28	795	795
$y_T \cdot \sin(\phi)$		301.36	371.28	444.11	511.02	510.59
$h_G \cdot \sin(\phi)$		676.19	800.00	917.72	1028.46	1027.60
s_a [1]		639.46	715.26	749.28	700.57	701.71
S_1	$10^{-3} \cdot m^2$	3784.30	2063.17	722.37	0	0
S_2				19855.65		
V_1		1513719.56	825269.57	288946.15	0	0
V_2	$10^{-6} \cdot m^3$			7942260.39		
V		9455979.95	7942260.39	8231206.54	7942260.39	7942260.39
b = 3.18 m; D = 1.59 m; h_G = 2.0 m; h_p = 1.09 m						
ϕ	[deg]	25	30	35	40	39.96 = ϕ_2 [1]
$h_G \cdot \sin(\phi)$	$10^{-3} \cdot$ m	845.24	1000	1147.15	1285.58	1284.51
s_a [1]		470.41	515.26	519.82	444.45	444.81
b = 3.18 m; D = 1.59 m; h_G = 2.5 m; h_p = 1.09 m						
ϕ	[deg]	25	30	35	40	39.96 = ϕ_2 [1]
$h_G \cdot \sin(\phi)$	$10^{-3} \cdot$ m	1056.55	1250.00	1433.94	1606.97	1605.63
s_a [1]		259.10	265.26	233.06	122.06	123.68

[1] see Figure 12, [2] see Figure 11b.

The 3rd phase begins with the left cylindrical float rising above the water surface $\phi_2 = 39.96$ deg (26), see Figure 11b, ending with the loss of buoyancy of the floating body ϕ_k [deg], see Table 8.

The coordinates of the centre of gravity $\{x_T, y_T\}$ [m, m] of the buoyancy force F_B [N] of the floating body during the 3rd phase of the deflection $\phi_2 \le \phi \le \phi_k$ [deg], at the float immersion dept (in the equilibrium state $\phi = 0$ deg) of the floating body $h_p = 1090$ mm, are given in Table 8.

Table 8. Coordinates of the centre of gravity $\{x_T, y_T\}$ [m, m] of the buoyancy force F_B [N] of the floating body during the 3rd phase of deflection $\phi_2 \le \phi \le \phi_k$ [deg] at immersion depth $h_p = 1090$ mm.

b = 3.18 m; D = 1.59 m; h_G = 1.6 m; h_p = 1.09 m							
ϕ	[deg]	45	50	55	60	65	63.15 = ϕ_k [1]
x_T					1590		
$x_T \cdot \cos(\phi)$	$10^{-3} \cdot$ m	1124.30	1022.03	911.99	795.00	671.96	718.13
y_T					795		
$y_T \cdot \sin(\phi)$		562.15	609.01	651.23	688.49	720.51	709.29

 doi:10.20944/preprints202604.1700.v1

$h_G \cdot \sin(\phi)$		1131.37	1225.67	1310.64	1385.64	1450.09	14.27.51
s_a[1]		555.08	405.37	252.57	97.85	–57.61	0
S_1	$10^{-3} \cdot m^2$	0					
S_2		19855.65					
V_1	$10^{-6} \cdot m^3$	0					
$V_2 = V$		7942260.39					
b = 3.18 m; D = 1.59 m; h_G = 2.0 m; h_p = 1.09 m							
ϕ	[deg]	45	50	55	52.84 = ϕ_k[1]		
$h_G \cdot \sin(\phi)$	$10^{-3} \cdot m$	1414.21	1532.09	1638.3	1593.90		
s_a[1]		272.24	98.95	–75.09	0		
b = 3.18 m; D = 1.59 m; h_G = 2.5 m; h_p = 0.5 m							
ϕ	[deg]	45	43.00 = ϕ_k[1]				
$h_G \cdot \sin(\phi)$	$10^{-3} \cdot m$	1767.77	1705.00				
s_a[1]		–81.32	0				

[1] see Figure 12.

2.4. Analytical Calculation of the Longitudinal Stability of a Floating Turntable with Cylindrical Floats

In the equilibrium state of the floating body, when the immersion of both floats of the floating body reaches the height $h_p = \frac{D}{2}$ [m], the area of the immersed surface of the left float S_1 [m^2] (for $\alpha = \pi = 180$ deg) can be expressed according to Figure 3 by relation (8).

The total S [m^2](2) immersion area of the two floats in the equilibrium state ($\phi = 0$ deg) of the floating body corresponds to the sum of the immersion areas S_1 [m^2] (8) and S_2 [m^2] (8) of the two cylindrical floats.

When calculating the stability and buoyancy of a floating body consisting of floats of circular cross-section by numerical solution according to the calculation program created in the Mathcad environment (version 14.0.0.163) [32], it is necessary to decompose the solution into two basic directions. These two directions result from the defined limiting angle ϕ_1 [deg] (13), which is defined as the tangent angle to the contours of the floats with respect to the horizontal plane, see Figure 3b.

The general angle ϕ [deg] of inclination of a floating body can take (with respect to the angle ϕ_1 [deg]) two values, described by the following states:

The 1st condition occurs when the tilt angle of the floating body ϕ [deg] is less than the angle ϕ_1 [deg] and at the same time greater than 0 deg, see (29). A general illustration of this state of float body tilt is given in Figure 4a.

$$0 < \phi \leq \phi_1[\text{deg}] \text{ or } 0 < \phi \leq \operatorname{asin}\left(\frac{D}{b}\right) [\text{deg}] \tag{29}$$

The 2nd condition occurs when the tilt angle is of the floating body ϕ [deg] is greater than the angle ϕ_1 [deg] and at the same time less than $\frac{\pi}{2} = 90$ deg, see (30), see Figure 7.

$$\phi_1 \leq \phi < 90 \text{ deg or } \operatorname{asin}\left(\frac{D}{b}\right) \leq \phi < \frac{\pi}{2} [\text{deg}] \tag{30}$$

Now both conditions (29) and (30) will be defined in more detail.

The condition for which the range of float angle is valid ϕ [deg] (29). A general illustration of this floating body roll condition is given in Figure 13a.

 doi:10.20944/preprints202604.1700.v1

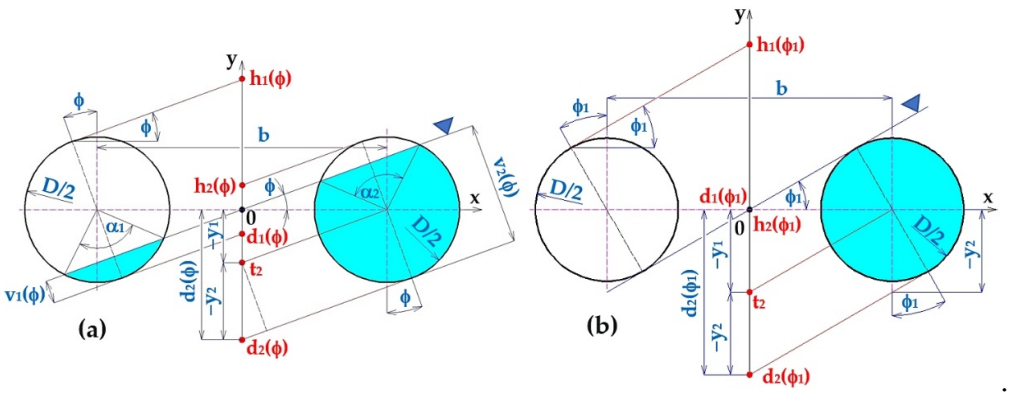

Figure 13. Deflection of the floating turntable by an angle ϕ [deg] **(a)** defined by the relation (32), **(b)** definition of the intersection distance $d_2(\phi)$[m] from the origin of the coordinate system.

The distance of the intersection $d_2(\phi)$ (this point is defined as the intersection of the tangent line with the vertical axis of symmetry of the floating body, drawn at an angle ϕ [deg] to the bottom of the right float) from the origin of the coordinate system, see Figure 13a, can be expressed by Equation (31).

$$d_2(\phi) = -y_1 - y_2 = -\frac{b}{2} \cdot \tan(\phi) - \frac{D}{2 \cdot \cos(\phi)} \text{ [m]} \tag{31}$$

where y_1 [m] is the length of the segment on the y-axis expressed by relation (32) using Figure 13a; y_2 [m] is the length of the segment on the y-axis expressed by relation (33) using Figure 13a.

$$\tan(\phi) = \frac{y_1}{b/2} \Rightarrow y_1 = \frac{b}{2} \cdot \tan(\phi) \text{ [m]} \tag{32}$$

$$\cos(\phi) = \frac{D/2}{y_2} \Rightarrow y_2 = \frac{D/2}{\cos(\phi)} \text{ [m]} \tag{33}$$

The intersection distance $h_1(\phi)$ (this point is defined as the intersection of the tangent of the left float of the floating body with the vertical axis, see Figure 13a, can be expressed by Equation (34).

$$h_2(\phi) = d_2(\phi) + 2 \cdot y_2 = -\frac{b}{2} \cdot \tan(\phi) + \frac{D}{2 \cdot \cos(\phi)} \text{[m]} \tag{34}$$

The distance of the intersection $d_1(\phi)$ (this point is defined as the intersection of the tangent line with the vertical axis of the floating body, drawn at an angle ϕ [deg] to the bottom of the left float) from the origin of the coordinate system, see Figure 13a; can be expressed by Equation (35).

$$d_1(\phi) = -h_2(\phi) = \frac{b}{2} \cdot \tan(\phi) - \frac{D}{2 \cdot \cos(\phi)} \text{ [m]} \tag{35}$$

The distance of the intersection $h_1(\phi)$; (this point is defined as the intersection of the tangent line with the vertical axis of symmetry of the floating body, drawn at an angle ϕ [deg] to the top of the left float) from the origin of the coordinate system, see Figure 13a; can be expressed by Equation (36).

$$h_1(\phi) = -d_2(\phi) = \frac{b}{2} \cdot \tan(\phi) + \frac{D}{2 \cdot \cos(\phi)} \text{[m]} \tag{36}$$

At an angle ϕ [deg] of inclination of the floating body, within the range defined by relation (29), the individual points (see Figure 13b) take on the following absolute magnitudes (37).

$$d_2(\phi)[m] < h_2(\phi)[m] \leq d_1(\phi)[m] < h_1(\phi)[m] \tag{37}$$

 doi:10.20944/preprints202604.1700.v1

The state of deflection of the floating body from the equilibrium position defined by assumption (29) must again be further decomposed into two states, described by the cases $h_p = \frac{D}{2}$ [m],$h_p < \frac{D}{2}$ [m] and $h_p > \frac{D}{2}$ [m].

ad 1a) The state of inclination of a floating body consisting of two cylindrical floats for which the angle ϕ [deg] of heeling is described by the relation (29) and the case where the position of the surface does not exceed the centre of the right float when the float is tilted, see Figure 14a.

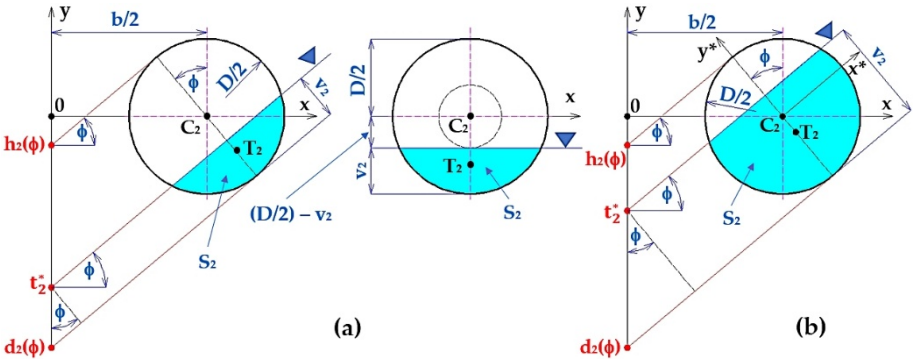

Figure 14. Right float of a floating body out of equilibrium, water level **(a)** does not exceed the centre C_2 of the float, **(b)** exceeds the centre C_2 of the float.

The point t_2^* (the intersection of the water surface with the vertical axis of symmetry of the floating body, when the floating body is deflected from the equilibrium position) lies in the interval $t_2^* \in \{d_2(\phi); h_2(\phi)\}$.

The height v_2 [m] of the submerged part of the right float (height of the circular section) of the floating body can be expressed according to Figure 14a by relation (38).

$$\cos(\phi) = \frac{v_2}{t_2^* - d_2(\phi)} \Rightarrow v_2 = [t_2^* - d_2(\phi)] \cdot \cos(\phi) \text{ [m]} \tag{38}$$

The surface area $S_2(t_2^*)$ [m^2] of the submerged part of the right cylindrical float can be expressed based on Figure 14a by relation (39).

$$S_2(t_2^*) = \int_{-\frac{D}{2}}^{-\frac{D}{2}+v_2} \left(\int_{-\sqrt{\left(\frac{D}{2}\right)^2 - y^2}}^{\sqrt{\left(\frac{D}{2}\right)^2 - y^2}} dx \right) \cdot dy \text{ [m}^2\text{]} \tag{39}$$

The position of the centre of gravity $T_2(t_2^*)$ [m] of the submerged part of the right cylindrical float can be expressed by relation (40) based on Figure 14a.

$$T_2(t_2^*) = \left\{ 0; \frac{\int_{-\frac{D}{2}}^{-\frac{D}{2}+[t_2^*-d_2(\phi)]\cdot\cos(\phi)} \left(\int_{-\sqrt{\left(\frac{D}{2}\right)^2 - y^2}}^{\sqrt{\left(\frac{D}{2}\right)^2 - y^2}} y.\, dx \right) \cdot dy}{S_2(t_2^*)} \right\} = \{0; y_2(t_2^*)\} \text{ [m; m]} \tag{40}$$

Position of the centre of gravity $T_2(\phi)$ [m] of the submerged part of the right float of a cylindrical floating body can be expressed, in the case where the plane of the water surface exceeds the centre of the float, based on Figure 14b, by the relation (41).

The centre of gravity $T_2(\phi)$ [m] of the immersed area S_2 [m^2] of the right float is on a line perpendicular to a line whose origin passes through a point t_2 and is inclined at an angle ϕ [deg], at

 doi:10.20944/preprints202604.1700.v1

a distance $b/2$ [m] from the centre C_2 of the float. The coordinates of the position of the centre of gravity T_2 [m] of the immersed area S_2 [m^2] of the right float can be expressed according to relation (41).

$$\{x_{T2}; y_{T2}\} = \left\{\frac{b}{2}; 0\right\} + k \cdot \frac{\{-\tan(\phi); 1\}}{\sqrt{1 + [\tan(\phi)]^2}} \text{ [m; m]} \tag{41}$$

where k [m] is the distance of the centre of gravity of the plunging surface of the right float from its centre, according to Figure 15c and relation (44) takes the size of y_2; $\frac{\{-\tan(\phi);1\}}{\sqrt{1+[\tan(\phi)]^2}}$ is the size of the unit vector in the direction of the axis y^* see Figure 14c and see Figure 15.

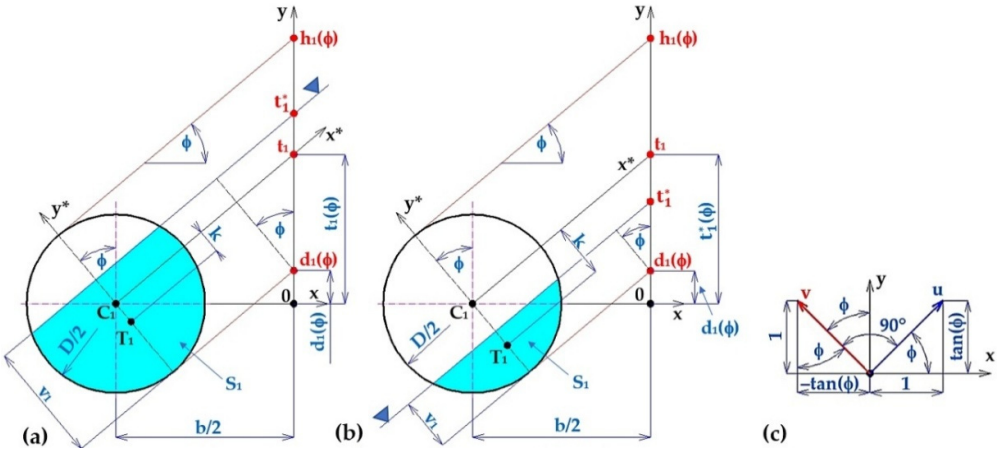

Figure 15. Left float of a floating body out of equilibrium, water level **(a)** over the centre C_1 of the left float; **(b)** exceeds the centre C_1 of the left float; **(c)** representation of the vectors.

Figure 15c shows the unit vector $u = \{1; \tan(\phi)\}$. From the mathematical analysis, the scalar product of two vector $u = (u_1, u_2)$ and vector $v = (v_1, v_2)$ can be described by relation (42), the result of the scalar product is a number. If the scalar product of two vectors is zero, these vectors are perpendicular to each other.

$$u \cdot v = u_1 \cdot v_1 + u_2 \cdot v_2 \tag{42}$$

If according to Figure 15c the vector "v" is to be perpendicular to the vector "u" its coordinates must be $v = \{-\tan(\phi); 1\}$ because then the condition that the scalar product of the two vectors is equal to zero is satisfied, see relation (43), and they are perpendicular to each other.

$$u \cdot v = u_1 \cdot v_1 + u_2 \cdot v_2 = 1 \cdot [-\tan(\phi)] + \tan(\phi) \cdot 1 \tag{43}$$

$$\begin{aligned} T_2(t_2^*) &= \left\{\frac{b}{2}; 0\right\} + y_2(t_2^*) \cdot \frac{(-\tan(\phi); 1)}{\sqrt{1 + [\tan(\phi)]^2}} = \\ &= \left\{\frac{b}{2} - \frac{\tan(\phi)}{\sqrt{1+[\tan(\phi)]^2}} \cdot y_2(t_2^*); \frac{1}{\sqrt{1+[\tan(\phi)]^2}} \cdot y_2(t_2^*)\right\} \text{ [m; m]} \end{aligned} \tag{44}$$

The heeling condition of a floating body consisting of two cylindrical floats for which the angle ϕ [deg] of heel is described by relation (29) and the surface plane exceeds the centre of the left float when the floating body is heeled, see Figure 15a. The point t_1^* (the intersection of the water surface with the vertical axis of symmetry of the floating turntable, when the turntable is deflected from the equilibrium position) lies in the interval $t_1^* \in \{d_1(\phi); h_1(\phi)\}$.

According to Figure 15a the height v_1 [m] of the submerged part of the left float (height of the circular section) can be determined by the relation (45).

$$\cos(\phi) = \frac{v_1(\phi)}{t_1^* - d_1(\phi)} \Rightarrow v_1(\phi) = [t_1^* - d_1(\phi)] \cdot \cos(\phi) \text{ [m]} \tag{45}$$

 doi:10.20944/preprints202604.1700.v1

The surface area $S_1(t_1^*)[m^2]$ of the submerged part of the left cylindrical float can be expressed by the relation (46) based on Figure 15a.

$$S_1(t_1^*) = \int_{-\frac{D}{2}}^{-\frac{D}{2}+v_1(\phi)} \left(\int_{-\sqrt{\left(\frac{D}{2}\right)^2 - y^2}}^{\sqrt{\left(\frac{D}{2}\right)^2 - y^2}} dx \right) \cdot dy = \\ = \int_{-\frac{D}{2}}^{-\frac{D}{2}+[t_1^* - d_1(\phi)]\cdot\cos(\phi)} \left(\int_{-\sqrt{\left(\frac{D}{2}\right)^2 - y^2}}^{\sqrt{\left(\frac{D}{2}\right)^2 - y^2}} dx \right) \cdot dy \, [m^2] \tag{46}$$

The position of the centre of gravity $T_1(t_1^*)$ [m] of the submerged part of the left float of the cylindrical floating body can be expressed by the relation (47) based on see Figure 15a.

$$T_1(t_1^*) = \left\{ 0; \frac{\int_{-\frac{D}{2}}^{-\frac{D}{2}+[t_1^* - d_1(\phi)]\cdot\cos(\phi)} \left(\int_{-\sqrt{\left(\frac{D}{2}\right)^2 - y^2}}^{\sqrt{\left(\frac{D}{2}\right)^2 - y^2}} y.\, dx \right) \cdot dy}{S_1(t_1^*)} \right\} = \{0; y_1(t_1^*)\} \, [m; m] \tag{47}$$

Position of the centre of gravity $T_1(\phi)$ [m] of the submerged part of the left cylindrical float of the float body can be expressed, in the case where the plane of the water surface exceeds the centre of the float, by Figure 15b, by the relation (48) a (49).

$$\{x_{T1}; y_{T1}\} = \left\{-\frac{b}{2}; 0\right\} + k \cdot \frac{\{-\tan(\phi); 1\}}{\sqrt{1 + [\tan(\phi)]^2}} \, [m; m] \tag{48}$$

$$T_1(t_1^*) = \left\{-\frac{b}{2}; 0\right\} + y_1(t_1^*) \cdot \frac{\{-\tan(\phi); 1\}}{\sqrt{1 + [\tan(\phi)]^2}} = \\ = \left\{-\frac{b}{2} - \frac{\tan(\phi)}{\sqrt{1 + [\tan(\phi)]^2}} \cdot y_1(t_1^*); \frac{1}{\sqrt{1 + [\tan(\phi)]^2}} \cdot y_1(t_1^*)\right\} \, [m; m] \tag{49}$$

In case $h_p = \frac{D}{2}$ [m] when the right float is not completely submerged below the water surface and the left float is not above the water surface, i.e., $\phi < \phi_1$ [deg], the immersion depth of the right float can be $v_2(\phi)$ [m] and the left float $v_1(\phi)$ [m] can be expressed according to the relation (50).

$$v_1(\phi) = \frac{D}{2} - \frac{b}{2} \cdot \sin(\phi) \, [m]; \; v_2(\phi) = \frac{D}{2} + \frac{b}{2} \cdot \sin(\phi) \, [m] \tag{50}$$

The content of the submerged area $S_2(t_2^*)$ [m^2] of the right cylindrical float, and the content of the submerged area $S_1(t_2^*)$ [m^2] of the left float, see Figure 13a, can be expressed for $\phi \le \phi_1 =$ 30 deg(13), by relation (39).

The position of the centre of gravity $T_1(t_1^*)$ [m] of the immersed surface $S_1(t_2^*)$ [m^2] of the left float of the floating body can be expressed by relation (49). The position of the centre of gravity $T_2(t_2^*)$ [m] of the immersed surface $S_2(t_2^*)$ [m^2] of the right float of the floating body, see Figure 13a, can be expressed by relation (44).

The coordinates of the centre of gravity $\{x_{T12}, y_T\}$ [m, m] of the floating body buoyancy force during the first phase of the deflection $0 \le \phi \le \phi_1$ at the float immersion depth $h_p = 795$ mm, expressed according to relations (44) and (49), are given in Table 9.

 doi:10.20944/preprints202604.1700.v1

Table 9. Coordinates of the centre of gravity $\{x_{T12}, y_T\}$ [m, m] of the buoyancy force of the floating body during phase 1 of the deflection, at the depth of immersion $h_p = 795$ mm.

b = 3.18 m; D = 1.59 m; h_p = 0.795 m								
ϕ	[deg]	0	5	10	15	20	25	30 = ϕ_1
x_{T1} (49)		−1590	−1553.97	−1504.77	−1442.83	−1369.13	−1285.07	−1192.5
x_{T2} (44)		1590	1613	1623.71	1623.59	1614.92	1601.28	1590
x_{T12}[1]		0	379.17	737	1053.74	1312.36	1498.29	1590
y_{T1} (49)	10^{-3}	−337.41	−411.87	−483.39	−549.23	−606.84	−653.92	688.49
y_{T2} (44)	· m	−337.41	−262.88	−191.2	−125.36	−68.47	−24.2	0
y_{T12}[1]		−337.41	−320.92	−274.02	−204.13	−123.06	−46.67	0
$y_T = h_p - y_{T12}$[1]		457.59	474.08	520.98	590.87	671.94	748.33	795
$S_1(t_1^*)$ (46)		9927.83	7735.65	5627.75	3689.87	2013.25	708.50	0
$S_2(t_2^*)$ (39)	10^{-4}	9927.83	12120.00	14227.91	16165.78	17842.40	19147.15	19855.65
$S = S_1(t_1^*) + S_2(t_2^*)$ (2)	· m^2				19855.65			

[1] see Table 1 and Appendix to the article No. 5 (Chapter I).

The coordinates of the center of gravity $\{x_T, y_T\}$ [m, m] of buoyant force F_B [N] of the floating body during the deflection $0 \le \phi \le \phi_2$ [deg] at different immersion depths h_p[m] are presented in Figure 16.

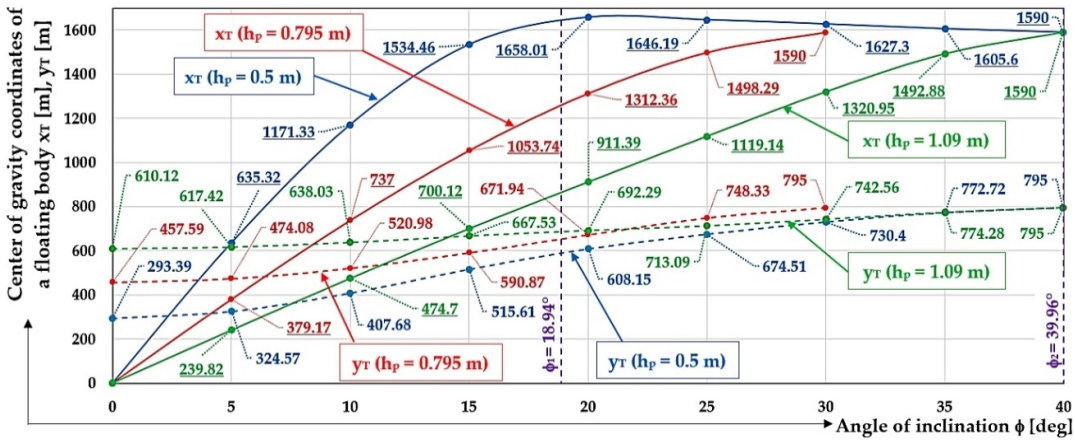

Figure 16. Coordinates of the centre of gravity $\{x_T, y_T\}$ [m, m] buoyancy forces of the floating body during deflection $0 \le \phi \le \phi_2$ at immersion depth h_p [m].

In case $h_p < \frac{D}{2}$ [m] when the port float is not completely above the water surface, i.e., $\phi < \phi_1$ [deg], the immersion depth of the right float can be $v_2(\phi)$ [m] and the left float $v_1(\phi)$ [m] can be expressed according to the relation (51).

$$v_1(\phi) = [t_2^* - d_1(\phi)] \cdot \cos(\phi)\ [m];\ v_2(\phi) = [t_2^* - d_2(\phi)] \cdot \cos(\phi)\ [m]. \quad (51)$$

for $t_2^* = h_p - \frac{D}{2}$ [m].

The area content of the submerged surface $S_2(t_2^*)$ [m^2], see Figure 14a, of the right cylindrical float can be expressed for $\phi \le \phi_1 = 18.94$ deg (16), (18) by relation (39). The submerged area $S_1(t_2^*)$ [m^2], see Figure 15b, of the left cylindrical float can be expressed for $\phi \le \phi_1 = 18.94$ deg (16) by relation (46).

 doi:10.20944/preprints202604.1700.v1

The position of the centre of gravity $T_1(t_1^*)$ [m] of the immersed surface $S_1(t_2^*)$ [m^2] of the left float of the floating body can be expressed by Equation (47). The position of the centre of gravity $T_2(t_2^*)$ [m] of the immersed surface $S_2(t_2^*)$ [m^2] of the right float of a floating body can be expressed by Equation (40).

The coordinates of the centre of gravity $\{x_{T12}, y_T\}$ [m, m] of the buoyancy force of the floating body during the first phase of the deflection $0 \le \phi \le \phi_1$ at the float immersion depth $h_p = 500$ mm, expressed according to relations (44) and (49), are given in Table 10.

Table 10. Coordinates of the centre of gravity $\{x_{T12}, y_T\}$ [m, m] of the buoyancy force of the floating body during phase 1 of the deflection, at the depth of immersion $h_p = 500$ mm.

b = 3.18 m; D = 1.59 m; h_p = 0.5 m						
ϕ	[deg]	0	5	10	15	18.94 = ϕ_1
x_{T1}(49)		−1590	−1539.38	−1475.53	−1399.48	−1659.32
x_{T2} (44)		1590	1626.85	1649.95	1659.92	1590
x_{T12} [1]		0	635.32	1171.33	1534.46	1590
y_{T1} (49)	$10^{-3} \cdot$ m	−501.61	−578.53	−649.18	−711.02	0
y_{T2} (44)		−501.61	−421.15	−339.97	−260.93	0
y_{T12}		−501.61	−470.43	−387.32	−279.39	−295
$y_T = (D/2) - y_{T12}$ [1]		293.39	324.57	407.68	515.61	500
$S_1(t_1^*)$ (46)		5347.31	3407.82	1753.75	510.21	0
$S_2(t_2^*)$ (39)	$10^{-4} \cdot m^2$	5347.31	7474.36	9698.60	11931.82	10694.62
$S = S_1(t_1^*) + S_2(t_2^*)$		10694.62	10882.18	11452.35	12442.03	10694.62

[1] see Table 3 and Appendix to the article No. 5 (Chapter II(a)).

In case $h_p < \frac{D}{2}$ [m] when the port float is completely above the water surface, i.e., $\phi_1 \le \phi \le \phi_2$ [deg], the immersion depth of the right float can be $v_2(\phi)$ [m] can be expressed by the relation (51).

The area content of the submerged surface $S_2(t_2^*)$ [m^2], see Figure 14a, of a right cylindrical float can be expressed for $\phi_1 \le \phi \le \phi_2$ [deg](21) by relation (39).

The position of the centre of gravity $T_2(t_2^*)$ [m] of the immersed surface $S_2(t_2^*)$ [m^2] of the right float of a floating body can be expressed by Equation (40).

The coordinates of the centre of gravity $\{x_{T12}, y_T\}$ [m, m] of the floating body buoyancy force during the second phase of the deflection $\phi_1 \le \phi \le \phi_2$ at the float immersion depth $h_p = 500$ mm, expressed according to relations (44) and (49), are given in Table 11.

Table 11. Coordinates of the centre of gravity $\{x_{T12}, y_T\}$ [m, m] of the buoyancy force of the floating body during phase 2 of the deflection, at the depth of immersion $h_p = 500$ mm.

b = 3.18 m; D = 1.59 m; h_p = 0.5 m						
ϕ	[deg]	20	25	30	35	39.96 = ϕ_2
x_{T1}				0		
x_{T2} (44) = x_{T12}		1658.01	1646.19	1627.30	1605.60	1590
y_{T1}	$10^{-3} \cdot$ m			0		
y_{T2}(44) = y_{T12}		−186.85	−120.49	−64.60	−22.28	0
$y_T = h_p - y_{T12}$		608.15 [1]	674.51 [2]	730.40 [2]	772.72 [2]	795 [2]
S_1	$10^{-4} \cdot m^2$			0		
$S = S_2(t_2^*)$ (39)		14085.97	16071.36	17792.49	19133.3	19855.37

 doi:10.20944/preprints202604.1700.v1

[1] see Table 3; [2] see Table 4 and Appendix to the article No. 5 (Chapter II(b)).

For the case $h_p > \frac{D}{2}$ [m], where the right float is not completely submerged below the water surface, i.e., $\phi \leq \phi_1$ [deg], the submergence depth of both the right float $v_2(\phi)$ [m] and the left float $v_1(\phi)$ [m] can be expressed by relation (51).

The area content of the submerged surface $S_2(t_2^*)$ [m^2], see Figure 14a, of a right cylindrical float can be expressed for $\phi \leq \phi_1 = 18.94$ deg (25) by relation (39). The submerged area $S_1(t_2^*)$ [m^2], see Figure 15b, of the left cylindrical float can be expressed for $\phi \leq \phi_1 = 18.94$ deg (25) by relation (46).

The position of the centre of gravity $T_1(t_1^*)$ [m] of the immersed surface $S_1(t_2^*)$ [m^2] of the left float of the floating body can be expressed by Equation (47). The position of the centre of gravity $T_2(t_2^*)$ [m] of the immersed surface $S_2(t_2^*)$ [m^2] of the right float of a floating body can be expressed by Equation (40).

The coordinates of the centre of gravity $\{x_{T12}, y_T\}$ [m, m] of the buoyant body buoyancy force during the first phase of the deflection $0 \leq \phi \leq \phi_1$ at the float immersion depth $h_p = 1090$ mm, expressed according to relations (44) and (49), are given in Table 12.

Table 12. Coordinates of the centre of gravity $\{x_{T12}, y_T\}$ [m, m] of the buoyancy force of the floating body during phase 1 of the deflection, at the depth of immersion $h_p = 1090$ mm.

b = 3.18 m; D = 1.59 m; h_p = 1.09 m						
ϕ	[deg]	0	5	10	15	18.94 $= \phi_1$
x_{T1} (49)	$10^{-3} \cdot m$	–1590	–1567.76	–1532.76	–1484.72	–1437.87
x_{T2} (44)		1590	1600.49	1601.09	1595.02	1590
x_T[1]		0	239.82	474.70	700.12	868.15
y_{T1} (49)		–184.88	–254.54	–324.62	–392.91	–443.32
y_{T2} (44)		–184.88	–119.87	–62.89	–18.75	0
y_{T12}		–184.88	–177.58	–156.97	–127.47	–105.69
$y_T = \frac{D}{2} - y_{T12}$[1]		610.12	617.42	638.03	667.53	689.31
$S_1(t_1^*)$ (46)	$10^{-4} \cdot m^2$	14508.35	12381.3	10157.06	7923.84	6215.35
$S_2(t_2^*)$ (39)		14508.35	16447.84	18101.92	19345.46	19855.67
$S = S_1(t_1^*) + S_2(t_2^*)$		29016.7	28829.15	28258.97	27269.30	26071.02

[1] see Table 6 and Appendix to the article No. 5 (Chapter III(a)).

In case $h_p > \frac{D}{2}$ [m] when the right float is completely submerged under the water surface, i.e., $\phi_1 \leq \phi \leq \phi_2$ [deg], the immersion depth of the left float can be $v_1(\phi)$ [m] can be expressed by the relation (51).

The area content of the submerged surface $S_1(t_2^*)$ [m^2], see Figure 14a, of the left cylindrical float can be expressed for $\phi_1 \leq \phi \leq \phi_2$ [deg] (21) by relation (46).

The position of the centre of gravity $T_1(t_1^*)$ [m] of the immersed surface $S_1(t_1^*)$ [m^2] of the left float of the floating body can be expressed by Equation (49).

The coordinates of the centre of gravity $\{x_{T12}, y_T\}$ [m, m] of the buoyant body buoyancy force during the second phase of the deflection $\phi_1 \leq \phi \leq \phi_2$ at the float immersion depth $h_p = 1090$ mm, expressed according to relations (44) and (49), are given in Table 13.

 doi:10.20944/preprints202604.1700.v1

Table 13. Coordinates of the centre of gravity $\{x_{T12}, y_T\}$ [m, m] of the buoyancy force of the floating body during phase 2 of the deflection, at the depth of immersion $h_p = 1090$ mm.

b = 3.18 m; D = 1.59 m; h_p = 1.09 m						
ϕ	[deg]	20	25	30	35	39.96 $= \phi_2$
x_{T2} (44)				1590		
x_{T1} (49)		–1423.97	–1351.39	–1268.37	–1176.71	–1079.44
x_{T12}		911.39 [1]	1119.14 [2]	1320.95 [2]	1492.88 [2]	1590 [2]
y_{T1} (49)	$10^{-3} \cdot$ m	–456.17	–511.7	–557.09	–590.24	–609.39
y_{T2} (44)				0		
y_{T12}		–456.17	–511.7	–557.09	–590.24	–609.39
$y_T = \frac{D}{2} - y_{T12}$		692.29 [1]	713.09 [2]	742.56 [2]	774.28 [2]	795 [2]
$S_1(t_1^*)$ (46)		5769.7	3784.30	2063.18	722.37	0
$S_2(t_2^*) = S_0$ (52)	$10^{-4} \cdot$ m^2			19855.67		
$S = S_1(t_1^*) + S_2(t_2^*)$ (39)		25625.36	23639.97	21918.84	20578.04	19855.67

[1] see Table 6; [2] see Table 7 and Appendix to the article No. 5 (Chapter III(b)).

The immersion area S_0 [m^2] of the entire right float of the floating body can be expressed according to (52).

$$S_0 = \int_{-\frac{D}{2}}^{\frac{D}{2}} \left(\int_{-\sqrt{\left(\frac{D}{2}\right)^2 - y^2}}^{\sqrt{\left(\frac{D}{2}\right)^2 - y^2}} dx \right) \cdot dy \ [m^2] \quad (52)$$

The 2nd phase begins with the moment of total emergence of the left right float ($\phi = \phi_1$ [deg]), and the right float, the floating body, and ends with loss of stability ($\phi = \phi_k$ [deg]).

Since, from the tilt angle $\phi_1 = \text{asin}\left(\frac{D}{b}\right)$ [deg] of the floating body, at the immersion depth $h_p = \frac{D}{2}$ [m] the right float of the floating body is completely immersed $S_2 = S_0$ [m^2] (Figure 7) and the surfaced area of the left float S_1 [m^2] acquires (with respect to the initial immersion depth $h_p = \frac{D}{2}$ [m]) an area $S_1 = S_0$ [m^2] (Figure 7 as the floating body is further tilted ($\phi > \phi_1$ [deg]). The position of the centre of gravity $\{x_{T2}; y_{T2}\}$ [m; m] of the immersed surface S_2 [m^2] of the right float of the floating body can be expressed according to Table 2.

Starting from the angle of inclination ϕ_2 [deg] (21) of the floating body, the right float of the floating body is fully submerged $S_2 = S_0$ [m^2] (52) at the immersion depth $h_p < \frac{D}{2}$ [m]. The position of the centre of gravity $\{x_{T2}; y_{T2}\}$ [m; m] of the immersed surface S_2 [m^2] of the right float of the floating body can be expressed according to Table 5.

From the angle of inclination ϕ_2 [deg] (28) of the floating body, the right float of the floating body is fully submerged $S_2 = S_0$ [m^2] (52) at the depth of immersion $h_p > \frac{D}{2}$ [m]. The position of the centre of gravity $\{x_{T2}; y_{T2}\}$ [m; m] of the immersed surface S_2 [m^2] of the right float of the floating body can be expressed according to Table 8.

3. Results

Verification of the buoyancy of the floating body in laboratory conditions was carried out on a test machine, whose 3D model created in the SolidWorks software environment (version Premium 2012×64, edition SP5.0) [33] is presented in Figure 17. The testing machine consists of a watertight tank 1 and a floating body 2 (which consists of two floats made of PLEXI pipe of 80/72 mm

 doi:10.20944/preprints202604.1700.v1

outer/internal diameter [34], length 200 mm and two connecting parts 4), which is mechanically attached to two force transducers 3, type MCF-100 N [35].

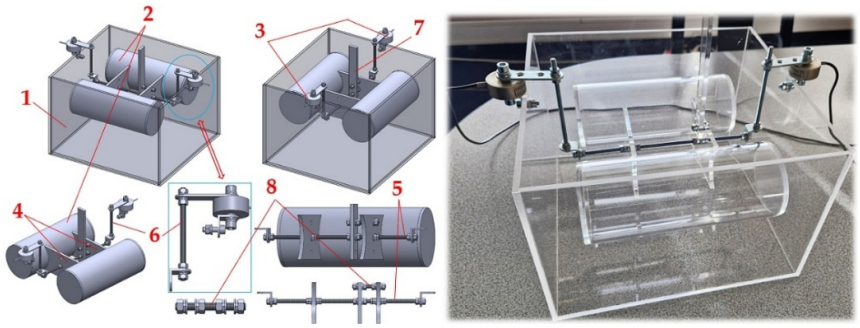

Figure 17. 3D model of a laboratory device to determine the buoyancy of a floating body. 1 – tank, 2 – floating body, 3 –- force transducer, 4 – float connecting part, 5 – axis, 6 – connecting assembly of axis with force transducer, 7 – PLEXI plate, 8 – connecting element.

According to Archimedes' law, the volume $V\,[m^3]$ of the floating body of the testing machine of mass $m_{FB}\,[kg]$ is immersed below the water surface. The floating body is buoyed by a force equal to the gravity of a fluid of the same volume as the submerged part of the floating body $V\,[m^3]$.

In the equilibrium state of the floating body of the test machine (angle $\phi = 0$ deg) of mass $m_{FB} = 0.746$ kg, the frontal surfaces of both floats (diameter $D\,[m]$ and length of one float and $[m]$, see Figure 2) of the floating body are submerged below the water surface by the size $S\,[m^2]$. If the floating body is designed so that its centre of gravity lies on the vertical axis of the axis of symmetry of the floating body, see Figure 18, then the horizontal axes of both floats of circular cross-section are parallel to the water surface.

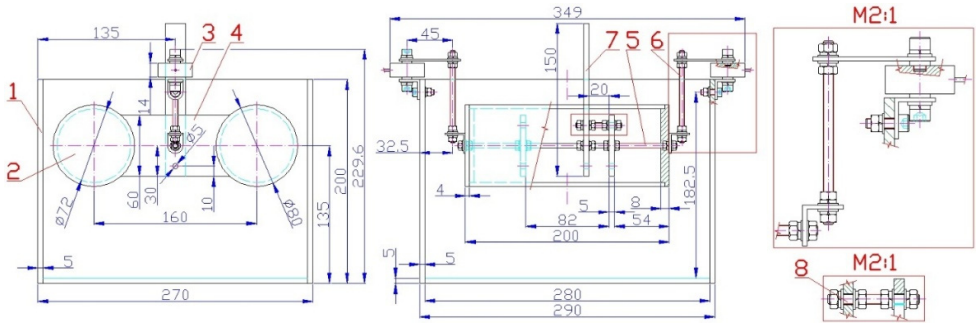

Figure 18. Basic dimensions of the testing machine. 1 – tank, 2 – floating body, 3 – force transducer [35], 4 – float connecting part, 5 – axis, 6 – connecting assembly of axis with force transducer, 7 – PLEXI plate, 8 – connecting element.

The total immersion area of a floating body $S\,[m^2]$ (53) is given by the sum of the immersion areas of the two floats $S = S_1 + S_2\,[m^2]$. Assuming that $S_1 = S_2\,[m^2]$ may be (with known value $S_1\,[m^2]$ and the diameter of the float $D\,[m]$) calculated in the Mathcad software environment (version 14.0.0.163) [32] by the instruction "Given–Find" the central angle $\alpha\,[deg]$ of the immersed area (circular segment) of one float from relation (54) and the depth $h_{p(m)}\,[m]$ of the immersion of the float (height of the circular segment) from relation (55).

$$\rho \cdot V = \rho \cdot S \cdot a = m_{FB} \Rightarrow S = \frac{m_{FB}}{\rho \cdot a} = \frac{0.746}{1000 \cdot 0.2} = 37.3 \cdot 10^{-4}\ m^2 \tag{53}$$

$$S_1\left(=\frac{S}{2}\right) = \frac{1}{2} \cdot \left(\frac{D}{2}\right)^2 \cdot [\alpha - \sin(\alpha)]\ [m^2] \Rightarrow \alpha = 156.46\ deg \tag{54}$$

 doi:10.20944/preprints202604.1700.v1

$$S_1 = \left(\frac{D}{2}\right)^2 \cdot \operatorname{acos}\left(\frac{\frac{D}{2} - h_{p(m)}}{\frac{D}{2}}\right) - \left(\frac{D}{2} - h_{p(m)}\right) \cdot \sqrt{2 \cdot h_{p(m)} \cdot \frac{D}{2} - h_{p(m)}^2}\ [m^2] \Rightarrow h_{p(m)} = 31.84\ \text{mm} \quad (55)$$

A buoyancy force $F_{B(m)}$ [N] (56) is exerted on the floating body of the test machine, consisting of cylindrical floats of diameter $D = 80$ mm and length $a = 200$ mm, at the immersion depth $h_{p(m)} = 31.84$ mm, see Figure 19a,b.

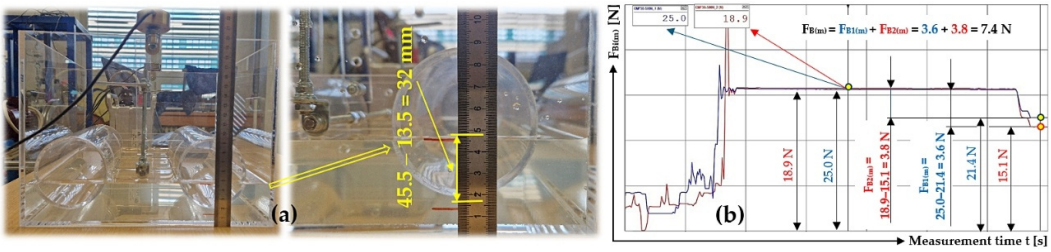

Figure 19. (a) plunging $h_{p(m)}$[m] of the floating body by its own mass m_{FB}[kg], **(b)** buoyancy force $F_{B(m)}$ [N] of a floating body by its own mass m_{FB}[kg].

$$F_{B(m)} = \rho \cdot S \cdot a \cdot g = 1000 \cdot 37.3 \cdot 10^{-4} \cdot 20 \cdot 10^{-3} \cdot g = 7.32\ \text{N} \quad (56)$$

A load sensor cable equipped with a D-Sub plug 4 was plugged into the socket of the measuring module BR4–D 4 [36] of the strain gauge apparatus DS NET during the laboratory measurements, see Figure 20. A PC 8 (ASUS K72JR–TY131 laptop) was connected to the DS NET strain gauge 6 using a network cable with RJ–45 connectors 7 at both ends.

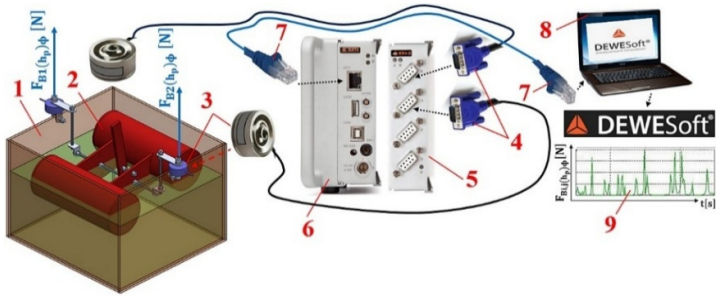

Figure 20. Measurement chain using DS NET to sense tensile forces $F_{Bi,j(h_p)\phi}$ [N]. 1 – tank, 2 – floating body, 3 – force sensor [35], 4 – D–Sub plug, 5 – measuring module.

With a known magnitude h_p [m] of the floats of the floating body at the equilibrium state ($\phi = 0$ deg) below the water surface, the floating body was deflected in the longitudinal direction by a known magnitude of angle ϕ [deg] through PLEXI plate 7. When the floating body was deflected out of its equilibrium state, the magnitudes of the buoyancy forces were detected by force transducers 3, see Figure 20, $F_{Bi,j(h_p)\phi}$ [N] (where "i" is the force transducer number, "j" is the measurement number).

The results of the experimental measurements of the buoyancy force $F_{Bi,j(h_p)\phi}$ [N] at the depth of immersion of the floating body of the testing machine $h_p = 20$ mm below the water surface and the known value of the longitudinal deflection of the floating body from the equilibrium state ϕ [deg] are shown in Table 14.

 doi:10.20944/preprints202604.1700.v1

Table 14. Buoyancy force $F_{Bi,j(20)\phi}$ [N] at the depth of submergence of the floating body $h_p = 20$ mm and longitudinal deflection of the floating body from the equilibrium state ϕ [deg].

h_p [10^{-3}m]	ϕ [deg]		0	10	20	30	40	50	60
		j							
20	$F_{B1,j(20)\phi}$[N]	1	1.90 [1]	2.21 [2]	3.14 [2]	3.65 [2]	4.54 [2]	4.91 [2]	4.92 [2]
		2 [3]	1.91	2.20	3.12	3.66	4.56	4.92	4.93
		3 [4]	1.91	2.21	3.15	3.67	4.54	4.93	4.92
	$F_{B1(20)\phi}$ [N]		1.91	2.21	3.14	3.66	4.55	4.92	4.92
	$\kappa_{1(5\%,3)\phi}$ [N]		± 0.02	± 0.02	± 0.04	± 0.03	± 0.03	± 0.03	± 0.02
h_p [10^{-3}m]	ϕ [deg]		0	10	20	30	40	50	60
		j							
20	$F_{B2,j(20)\phi}$[N]	1	1.90 [1]	2.19 [2]	3.13 [2]	3.66 [2]	4.55 [2]	4.93 [2]	4.93 [2]
		2 [3]	1.93	2.20	3.16	3.65	4.54	4.93	4.92
		3 [4]	1.93	2.20	3.14	3.64	4.55	4.92	4.93
	$F_{B2(20)\phi}$ [N]		1.92	2.20	3.14	3.65	4.55	4.93	4.93
	$\kappa_{2(5\%,3)\phi}$ [N]		± 0.05	± 0.02	± 0.04	± 0.03	± 0.02	± 0.02	± 0.02
$h_p = 20$ mm	ϕ [deg]		0	10	20	30	40	50	60
$F_{B(20)\phi} = F_{B1(20)\phi} + F_{B2(20)\phi}$ [N]			3.83	4.41	6.28	7.31	9.10	9.85	9.85

[1] see Figure 21a; [2] see Figure 21b; [3] see Figure 22a; [4] see Figure 22b.

Figure 21a shows the measured values of buoyancy forces $F_{Bj(h_p)0}$ [N] , by force sensors MCF-100 N, with floats of circular cross-section not submerged below the water surface and at float submergence depth $h_p = 20$ mm floats, at the angle of deflection $\phi = 0$ deg.

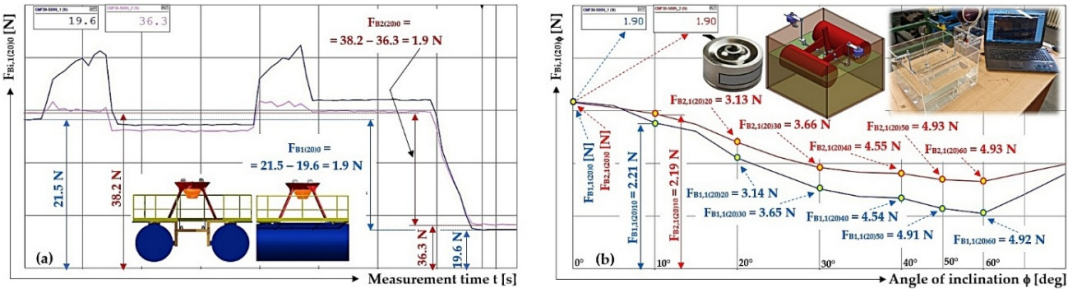

Figure 21. Measured buoyancy force waveform **(a)** $F_{Bj(h_p)0}$ [N] of the non-immersed and immersed $h_p = 20$ mm floating body, **(b)** $F_{Bi,1(20)\phi}$ [N] when submerged $h_p = 20$ mm and deflection $\phi = 0 \div 60$ deg of the floating body from the equilibrium position.

Figure 21b shows the measured values of buoyancy forces $F_{Bi,1(20)\phi}$ [N] by force sensors MCF–100 N, at a immersion depth of $h_p = 20$ mm of the floats below the water surface, with gradual deflection $\phi = 0 \div 60$ deg of the floating body of the testing machine.

Figure 22 shows the measured values of buoyancy forces $F_{Bi,j(20)\phi}$ [N] by force sensors MCF–100 N, at the immersion depth $h_p = 20$ mm of the floats below the water surface, with gradual deflection $\phi = 0 \div 60$ deg of the floating body of the testing machine.

 doi:10.20944/preprints202604.1700.v1

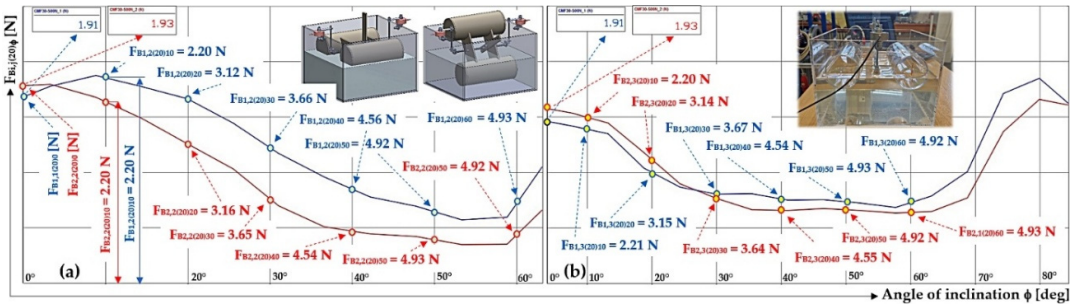

Figure 22. Measured buoyancy force during deflection $\phi = 0 \div 60$ deg of the floating body from the equilibrium position **(a)** $F_{Bi,2(20)\phi}$ [N], **(b)** $F_{Bi,3(20)\phi}$ [N].

From three times $(n = 3)$ repeated measurements under the same technical conditions, the arithmetic mean $F_{Bi(h_p)\phi}$ [N] and the marginal error $\kappa_{i(\beta,n)\phi}$ [N] (57) were calculated according to Student's distribution [38].

$$\kappa_{i(\beta,n)\phi} = t_{\beta,n} \cdot \bar{s}\ [N] \tag{57}$$

where $t_{\beta,n}$ [−] is the Student's coefficient (for the chosen risk $\beta = 5\%$ and the number of measured values $n = 3$ can be determined according to [38] $t_{\beta,n} = t_{5\%,3} = 4.3$); $\bar{s}$ [N] is the standard deviation of the arithmetic mean (58).

$$\bar{s} \approx \frac{5}{4} \cdot \frac{\sum_{j=1}^{3} \left| F_{Bi,j(h_p)\phi} - F_{Bi(h_p)\phi} \right|}{n \cdot \sqrt{n-1}}\ [N] \tag{58}$$

From the measured mean value of the buoyancy force $F_{B(h_p)\phi}$ [N] according to the relation (59) to express the total immersed area of the floats $S_{(h_p)\phi}$ [m²] of the floating body of the testing machine at the immersion depth h_p [m] and deflection angle ϕ [deg] of the floating body from the equilibrium state.

$$S_{(h_p)\phi} = \frac{F_{B(h_p)\phi}}{\rho \cdot a \cdot g}\ [m^2] \tag{59}$$

Table 15 shows the total immersed area of the floats $S_{(h_p)\phi}$ [m²] of the floating body of the testing machine at the immersion depth $h_p = 20$ mm and deflection angle ϕ [deg] of the floating body from the equilibrium state.

Table 15. Submerged area of floats $S_{(20)\phi}$ [m²] of the floating body of the testing machine at the immersion depth $h_p = 20$ mm and deflection angle ϕ [deg].

ϕ [deg]	0	10	20	30	40	50	60
$F_{B(20)\phi}$ [N] [1]	3.83	4.41	6.28	7.31	9.10	9.85	9.85
$S_{(20)\phi}\ [10^{-6} \cdot m^2]$	1952.76	2248.47	3201.91	3727.06	4639.71	5022.10	5022.10

[1] see Table 14.

The results of the experimental measurements of the buoyancy force $F_{Bi,j(h_p)\phi}$ [N] at the depth of immersion of the floating body of the testing machine $h_p = 40$ mm below the water surface and the known value of the longitudinal deflection of the floating body from the equilibrium state ϕ [deg] are shown in Table 16.

 doi:10.20944/preprints202604.1700.v1

Table 16. Submerged area of floats $S_{(20)\phi}$ [m^2] of the floating body of the testing machine at the immersion depth $h_p = 40$ mm and deflection angle ϕ [deg].

h_p [10^{-3}m]	ϕ [deg]		*0 ÷ 60*
		j	
40	$F_{B1,j(40)\phi}$[N]	1	4.9 [1]
		2	4.8
		3	4.9
	$F_{B1(40)\phi}$ [N]		4.9
	$\kappa_{1(5\%,3)\phi}$ [N]		± 0.2
h_p [10^{-3}m]	ϕ [deg]		*0 ÷ 60*
		j	
40	$F_{B,2j(40)\phi}$[N]	1	4.7 [1]
		2	4.7
		3	4.8
	$F_{B2(40)\phi}$ [N]		4.7
	$\kappa_{2(5\%,3)\phi}$ [N]		± 0.1
$h_p = 40$ mm	ϕ [deg]		*0 ÷ 60*
$F_{B(40)\phi} = F_{B1(40)\phi} + F_{B2(40)\phi}$ [N]			9.6
$S_{(40)\phi}\ \left[10^{-6} \cdot m^2\right]$			4894.64

[1] see Figure 23b.

Figure 23b shows the measured values of buoyancy forces $F_{Bi,1(40)\phi}$ [N] by force sensors MCF–100 N, at a immersion depth of $h_p = 40$ mm of the floats below the water surface, with gradual deflection $\phi = 0 \div 60$ deg of the floating body of the testing machine.

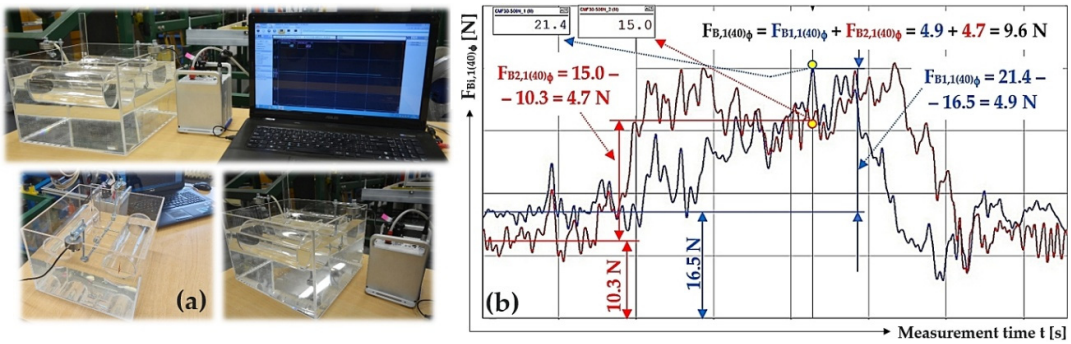

Figure 23. (a) realization of the testing machine, **(b)** measurement of the buoyancy force during deflection $\phi = 0 \div 60$ deg of the floating body from the equilibrium position $F_{Bi,2(40)\phi}$ [N].

The results of the experimental measurements of the buoyancy force $F_{Bi,j(h_p)\phi}$ [N] at the depth of immersion of the floating body of the testing machine $h_p = 60$ mm below the water surface and the known value of the longitudinal deflection of the floating body from the equilibrium state ϕ [deg] are shown in Table 17.

 doi:10.20944/preprints202604.1700.v1

Table 17. Submerged area of floats $S_{(20)\phi}$ [m^2] of the floating body of the testing machine at the immersion depth $h_p = 60$ mm and deflection angle ϕ [deg].

h_p [10^{-3}m]	ϕ [deg]		0	10	20	30	40	50	60
		j							
60	$F_{B1,j(60)\phi}$[N]	1	7.86 [1]	7.61 [2]	6.72 [2]	5.62 [2]	4.81 [2]	4.79 [2]	4.79 [2]
		2 [3]	7.92	7.59	6.75	5.70	4.94	4.74	4.71
		3 [4]	7.89	7.64	6.72	5.63	4.97	4.77	4.75
	$F_{B1(60)\phi}$ [N]		7.89	7.61	6.73	5.65	4.91	4.77	4.75
	$\kappa_{1(5\%,3)\phi}$ [N]		± 0.02	± 0.07	± 0.05	± 0.13	± 0.09	± 0.07	± 0.10
h_p [10^{-3}m]	ϕ [deg]		0	10	20	30	40	50	60
		j							
60	$F_{B,2j(60)\phi}$[N]	1	7.91 [1]	7.65 [2]	6.70 [2]	5.66 [2]	4.89 [2]	4.77 [2]	4.81 [2]
		2 [3]	7.86	7.61	6.74	5.69	4.93	4.80	4.74
		3 [4]	7.88	7.62	6.71	6.01	4.95	4.79	4.78
	$F_{B2(60)\phi}$ [N]		7.88	7.63	6.72	5.79	4.92	4.79	4.78
	$\kappa_{2(5\%,3)\phi}$ [N]		± 0.02	± 0.06	± 0.06	± 0.57	± 0.03	± 0.02	± 0.04
$h_p = 60$ mm	ϕ [deg]		0	10	20	30	40	50	60
$F_{B(60)\phi} = F_{B1(60)\phi} + F_{B2(60)\phi}$ [N]			15.77	15.24	13.45	11.44	9.83	9.56	9.53

[1] see Figure 24a; [2] see Figure 24b; [3] see Figure 25a; [4] see Figure 25b.

Figure 24a shows the measured values of buoyancy forces $F_{Bj,1(60)\phi}$ [N], by force sensors MCF-100 N, with floats of circular cross-section not submerged below the water surface and at float submergence depth $h_p = 60$ mm floats, at the angle of deflection $\phi = 0$ deg.

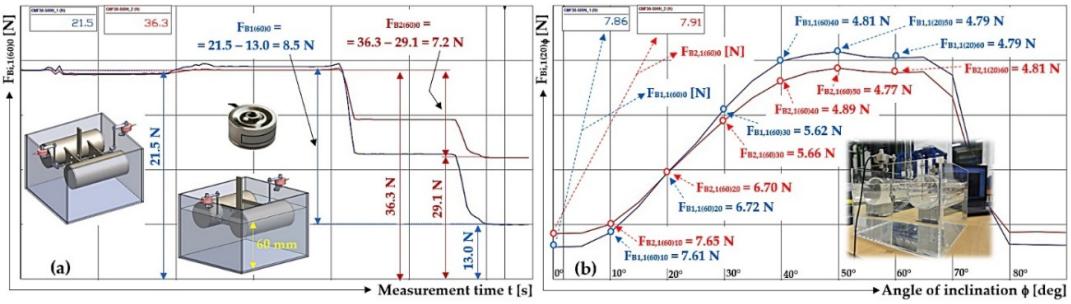

Figure 24. Measured buoyancy force waveform **(a)** $F_{Bj(h_p)0}$ [N] of the non-immersed and immersed $h_p = 60$ mm floating body, **(b)** $F_{Bi,1(60)\phi}$ [N] when submerged $h_p = 60$ mm and deflection $\phi = 0 \div 60$ deg of the floating body from the equilibrium position.

Figure 24b shows the measured values of buoyancy forces $F_{Bi,1(60)\phi}$ [N] by force sensors MCF–100 N, at a immersion depth of $h_p = 60$ mm of the floats below the water surface, with gradual deflection $\phi = 0 \div 60$ deg of the floating body of the testing machine.

Figure 25 shows the measured values of buoyancy forces $F_{Bi,j(60)\phi}$ [N] by force sensors MCF–100 N, at a immersion depth of $h_p = 60$ mm of the floats below the water surface, with gradual deflection $\phi = 0 \div 60$ deg of the floating body of the testing machine.

Preprints.org (www.preprints.org) | NOT PEER-REVIEWED | Posted: 23 April 2026 doi:10.20944/preprints202604.1700.v1

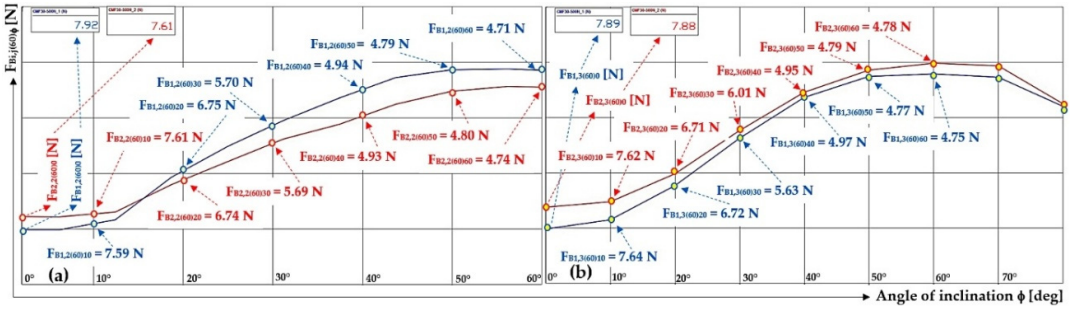

Figure 25. Measured buoyancy force during deflection $\phi = 0 \div 60$ deg of the floating body from the equilibrium position **(a)** $F_{Bi,2(60)\phi}$ [N], **(b)** $F_{Bi,3(60)\phi}$ [N].

Table 18 shows the total immersed area of the floats $S_{(h_p)\phi}$ [m^2] of the floating body of the testing machine at the immersion depth $h_p = 60$ mm and deflection angle ϕ [deg] of the floating body from the equilibrium state.

Table 18. Submerged area of floats $S_{(60)\phi}$ [m^2] of the floating body of the testing machine at the immersion depth $h_p = 60$ mm and deflection angle ϕ [deg].

ϕ [deg]	0	10	20	30	40	50	60
$F_{B(60)\phi}$ [N] [1]	15.77	15.24	13.45	11.44	9.83	9.56	9.53
$S_{(60)\phi}\ \left[10^{-6} \cdot m^2\right]$	8040.46	7770.24	6857.59	5832.78	5011.91	4874.24	4858.95

[1] see Table 18.

4. Discussion

The issue of longitudinal and transverse stability of floating belt conveyors using floating bodies with floats of circular cross-section [28,39] has not been comprehensively and systematically analysed so far, which is evidenced by the lack of relevant scientific articles and publications in this area.

In the presented paper, two methodological approaches are described to determine the position of the centre of gravity of the displacement of a floating body during its longitudinal deflection from the equilibrium state.

The first method (see Sections 2.1–2.3) is based on the graphical and numerical determination of the centre of gravity of the displacement of the floating body, which is complemented by the use of 3D modelling tools (e.g., SolidWorks [33] or Inventor). The computationally demanding and time-consuming analytical procedure for determining the position of the centre of gravity of the displacement when the body is deflected from its equilibrium position can be effectively replaced by determining the centre of gravity based on a volume model created in a CAD system environment.

The results obtained for the coordinates of the centre of gravity of the displacement $\{x_T; y_T\}$ [m; m] (i.e., the centre of buoyancy force F_B[N]) at each stage of the deflection of the floating body from the equilibrium state by a known magnitude of angle ϕ [deg], at three immersion depths h_p [m] (0.795; 0.5; 1.09) are given in Tables 1–8.

Maximum stability arm value $s_{and} = 997.98 - 10^{-3}$ m is achieved for cylindrical floats of diameter $D = 1.59$ m whose submergence below the water surface reaches exactly half the float diameter, i.e., $h_G = \frac{D}{2} = 0.795$ m, at an angle of heel $\phi = 25$ deg (see Table 1).

Maximum stability arm value $s_{and} = 1.24$ m is achieved for cylindrical floats of diameter $D = 1.59$ m whose submergence below the water surface does not exceed half the diameter, e.g., $h_G < \frac{D}{2} = 0.5$ m, at an angle of heel $\phi \approx 19$ deg (see Table 3).

 doi:10.20944/preprints202604.1700.v1

Maximum stability arm size $s_{and} = 701.01 - 10^{-3}$ m is achieved for cylindrical floats of diameter $D = 1.59$ m whose submergence below the water surface exceeds half the diameter, e.g., $h_G > \frac{D}{2} = 1.09$ m, at an angle of heel $\phi \approx 40$ deg (see Table 7).

The second method (see Section 2.4) is based on the analytical determination of the coordinates of the centre of gravity of the displacement of the floating body. The coordinates of the centre of gravity of the displacement are identical to the values of $\{x_T, y_T\}$ [m, m] determined by the "first method".

Table 9 presents the coordinates of the centre of gravity $\{x_{T12}, y_{12}\}$ [m, m] of the buoyancy force of the floating body during phase 1 of the deflection, at the depth of immersion $h_p = 795$ mm.

Table 10 presents the coordinates of the centre of gravity $\{x_{T12}, y_{12}\}$ [m, m] of the buoyancy force of the floating body during phase 1 of the deflectiion, and Table 11 presents the coordinates of the centre of gravity $\{x_{T12}, y_{12}\}$ [m, m] of the buoyancy force of the floating body during the 2nd phase of the deflection, at the depth of immersion $h_p = 500$ mm.

Table 12 presents the coordinates of the centre of gravity $\{x_{T12}, y_{12}\}$ [m, m] of the buoyancy force of the floating body during phase 1 of the deflection, and Table 13 presents the coordinates of the centre of gravity $\{x_{T12}, y_{12}\}$ [m, m] of the buoyancy force of the floating body during the 2nd phase of the yaw, at the depth of immersion $h_p = 1090$ mm.

The aim of the experimental tests carried out on laboratory equipment (see Figure 23a) was to determine the actual buoyancy force values based on direct measurements using force transducers [35], depending on the angle of ϕ [deg] inclination and at different levels of immersion h_p [m] of the floating body below the liquid surface [1].

Experimental measurements verified the correctness of the analytical determination of the position of the centre of gravity of the displacement of the floating body during its longitudinal deflection from the equilibrium position.

Based on Figures 21b and 22 the conclusion can be formulated that when the floating body is submerged below the surface by a value exceeding half of the float diameter (circular cross-section), the magnitude of the buoyancy force decreases with increasing angle of inclination.

When the floating body is immersed to a depth of half the diameter of the cylindrical floats, the buoyancy force remains constant, see Figure 23b. When a floating body is more or less submerged, the amount of buoyancy force changes with increasing angle of inclination, either decreasing or increasing depending on the specific submergence conditions.

Based on Figures 24b and 25, it can be concluded that when the floating body is submerged below the surface by a value not exceeding half of the float diameter (circular cross-section), the magnitude of the buoyancy force increases with increasing angle of inclination.

Future research directions in the area of floating conveyor belt buoyancy should also focus on a detailed analysis of the stability loss mechanisms in relation to the transverse stability of the floating body [40]. The key topic is to deepen the understanding of critical states, in which the transition from steady state to unsteady behaviour occurs due to changes in buoyancy distribution and metacentre shift during transverse deflection of the floating body [41].

Furthermore, it is appropriate to extend the research by experimental and numerical modelling of the dynamic response of floating conveyors to external loads, including the effects of waves, uneven loading and changes in embedment. Attention should also be paid to the influence of the geometrical parameters of the floats and their arrangement on the so-called "metacentric height" [2,28] and the overall lateral stability of the system.

Optimization of the structural design to increase the stability margin is also a promising area, especially through modifications of the shape of the floats, their mutual configuration and the weight distribution of the conveyor [21,25]. At the same time, the development of advanced computational methods can be recommended [7,18,19,22], which allow reliable prediction of stability limit states in real operating conditions.

 doi:10.20944/preprints202604.1700.v1

5. Conclusions

Floating belt conveyor routes, consisting of serially arranged belt conveyors, the end parts of which are mechanically fixed to floating bodies, are used for the continuous transport of extracted granular materials from the water environment. The paper focuses on the analytical determination of the position of the centre of gravity of the buoyancy force, the coordinates of which change depending on the longitudinal deflection of the floating body from the equilibrium position, while this body performs the function of the supporting element of individual conveyor belts.

The analysis of the individual phases of the deflection of the floating body, consisting of a pair of cylindrical floats with a circular cross-section, showed that the complete immersion of one of the floats occurs at a higher angle of inclination in the case when the floats are immersed in the initial equilibrium position to just half of their diameter.

The experimental verification was carried out on a laboratory machine, where the magnitude of the buoyancy force was measured using strain gauges during the gradual deflection of the floating body from the equilibrium position for three defined levels of immersion. The floating body used in the experiment consisted of a pair of cylindrical floats with a circular cross-section with a diameter of 80 mm.

The result of the work is a systematic methodological procedure for determining the position of the centre of gravity of the displacement (centre of buoyancy) when the floating body deviates from the equilibrium position, together with a methodology for calculating the stability arm as a key parameter for assessing the buoyancy and lateral stability of the structure.

Based on laboratory measurements, the behaviour of the buoyancy force as a function of the immersion depth was further quantified. It was found that the buoyancy force remains constant during deflection only at a immersion corresponding to half the float diameter. At lower immersion, the buoyancy force increases with increasing angle of bank, while at higher drafts, its magnitude decreases with increasing bank.

Author Contributions: Conceptualization, L.H.; methodology, L.H.; software, L.H. and L.K.; validation, L.H., P.K. and L.K.; formal analysis, L.H.; investigation, L.H.; resources, L.H. and P.K; data curation, L.H.; writing—original draft preparation, L.H.; writing—review and editing, L.H.; visualization, L.H.; supervision, L.H.; project administration, L.K.; funding acquisition, L.H. All authors have read and agreed to the published version of the manuscript.

Funding: This research was funded by The Ministry of Education, Youth and Sports (MEYS, MŠMT in Czech), grant number SP2026/001. The APC was funded by MSM: SV_2010 – Specifický výzkum VŠB-TUO.

Data Availability Statement: Measured data of buoyancy forces $F_{Bi,j(h_p)\phi}$ [N] (force sensors ESM30–100N [35]), listed in Tables 14, 16 and 17 and processed using DEWESoft X software, can be provided upon request after prior written agreement in ∗.XLSX (Microsoft Excel) format or in ∗.DXD (DEWESOFT X [37]).

Acknowledgments: I would like to express my sincere gratitude to all collaborators who contributed to this research by providing intellectual support, technical assistance, and specialized equipment. I also wish to thank VSB–Technical University of Ostrava for their financial support. This work has been supported by The Ministry of Education, Youth and Sports of the Czech Republic from the Specific Research Project SV 3402256 (SP 2026/001).

Conflicts of Interest: The authors declare no conflicts of interest. The funders had no role in the design of the study; in the collection, analyses, or interpretation of data; in the writing of the manuscript; or in the decision to publish the results.

Appendix A

Appendix A.1

– a PDF file named “Appendix A.1”.

 doi:10.20944/preprints202604.1700.v1

Appendix A.2

– a PDF file named "Appendix A.2".

Appendix A.3

– a PDF file named "Appendix A.3".

Appendix A.4

– a PDF file named "Appendix A.4".

Appendix A.5

– a XMCD file (created in Mathcad 2014 software, version version 14.0.0.163 [32]) named "Appendix A.5".

References

1. Hrabovsky, L. *Pásové dopravní trasy ve vodních pískovnách*, (In English: *Belt conveyor systems in sand and gravel quarries with water-filled pits*), 1rd ed.; VSB - Technical University of Ostrava: Ostrava, Czech Republic, 2010; p. 156. ISBN 8024823136. https://ceskadigitalniknihovna.cz/view/uuid:ba286a00-7495-11e8-87bd-005056827e52?page=uuid:cb42f540-8a06-11e8-9690-005056827e51&source=mzk.
2. Zadnik, B. *Stavba a opravy lodí*, (In English: *Shipbuilding and ship repair*), 1rd ed.; NADAS: Praha, Czech Republic, 1980; p. 461.
3. Floating conveyor belts. Available online: https://prosand.cz/stroje/plovouci-dopravnikove-pasy (accessed on 18. Marth 2021).
4. Floating conveyor belts. Available online: https://www.ffa-fiebig.de/index.php/en/belt-conveyors/floating-belt-conveyors. (accessed on 20. November 2025).
5. Vassalos, D.; Paterson, D. Towards unsinkable ships. *Ocean Engineering* **2021**, *232*, 109096. https://doi.org/10.1016/j.oceaneng.2021.109096.
6. Grochowalski, S.; Pawlowski, M. The safety of Ro-Ro vessels in the light of the probabilistic concept for standardizing unsinkability. *International Shipbuilding Progress* **1981**, *28*(319), pp. 63–72. https://doi.org/10.3233/ISP-1981-2831903.
7. Hrabovsky, L.; Nenicka, P.; Fries, J. Laboratory machine verification of force transmission provided by friction acting on the drive drum of a conveyor belt. *Machines* **2023**, *11*(5), p. 544. https://doi.org/10.3390/machines11050544.
8. Kassem, A.H. The legal aspects of seaworthiness: current law and development, Doctoral dissertation, Swansea University, 13. Marth 2006.
9. Chamlee, G.H. The absolute warranty of seaworthiness: a history and comparative study. *Mercer L. Rev.* **1973**, *24*, p. 519.
10. Padovan, A.V. The elements of seaworthiness in the context of marine insurance revisited. In Proceedings of the 4th International scientific conference on maritime LAW–ISCML Split 2023: Modern challenges of marine navigation (pp. 101–122), Split, Croatia (13–14 April 2023). https://iscml-split.com/wp-content/uploads/2024/04/zbornik_pomorsko-pravo_2023.pdf.
11. So, L.K.; Sooksripaisarnkit, P. Seaworthiness and autonomous ships: Legal implications in the 21st century. *Australian and New Zealand Maritime Law Journal* **2021**, *35*(1), pp. 21–30. https://search.informit.org/doi/epdf/10.3316/informit.514450668875220.
12. Girvin, S. The Obligation of Seaworthiness: Shipowner and Charterer. In Proceedings of the 25th Pan–American Conference of Naval Engineering, Copinaval, Peru, (5 October 2017). https://doi.org/10.1007/978-3-319-89812-4_37.
13. Gonzalez, M.M.; Sobrino, P.C.; Alvarez, R.T.; Casas, V.D.; Lopez, A.M.; Pena, F.L. Fishing vessel stability assessment system. *Ocean Engineering* **2012**, *41*, pp. 67-78. https://doi.org/10.1016/j.oceaneng.2011.12.021.
14. Umar, A.; Ahmad, S.; Datta, T.K. Stability analysis of a moored vessel. *Journal of Offshore Mechanics and Arctic. Engineering* **2004**, *126* (2), pp. 164–174. https://doi.org/10.1115/1.1710873.

 doi:10.20944/preprints202604.1700.v1

15. Leira, B. J.; Berntsen, P. I. B.; Aamo, O. M.; Sorensen, A. J. Reliability-based dynamic position control of floating vessels: a numerical and experimental study. *Ships and Offshore Structures* **2009**, *4*(3), pp. 207–214. https://doi.org/10.1080/17445300902836478.
16. Halyna, D. Vessel dynamic positioning system mathematical model. In Proceedings of the VIII International Science Conference – Modern technologies of human development, Bordeaux, France (6–8 November 2023). https://lib.udau.edu.ua:8443/server/api/core/bitstreams/6e7388ca-eda5-4aa2-9e03-db68b13bf9ae/content.
17. Michalik, P.; Dobransky, J.; Hrabovsky, L.; Petrus, M. Assessment of the Manufacturing Possibility of Thin-Walled Robotic Portals for Conveyor Worklace. *Advances in Science and Technology. Research Journal* **2018**, *12*(1), pp. 338–345. https://doi.org/10.12913/22998624/87063.
18. Francescutto, A.; Papanikolaou, A. D. Buoyancy, stability, and subdivision: from Archimedes to SOLAS 2009 and the way ahead. *Proceedings of the Institution of Mechanical Engineers, Part M: Journal of Engineering for the Maritime Environment* **2011**, *225*(1), pp. 17–32. https://doi.org/10.1177/14750902JEME238.
19. Ruponen, P. *Principles of ship buoyancy and stability*, 1rd ed.; Publisher: Helsinki, Finland, 2021; p. 174. https://aaltodoc.aalto.fi/server/api/core/bitstreams/a9de4444-baa0-4009-96a6-88a96b8e669a/content.
20. Martic, I.; Degiuli, N.; Grlj, C.G.; Borcic, K.; Andrisic, J.; Lalovic, I. Impact of the longitudinal center of buoyancy on the total resistance of a passenger ship. *Journal of marine science and engineering* **2024**, *12*(10), 1749. https://doi.org/10.3390/jmse12101749.
21. Spyrou, K.J. The stability of floating regular solids. *Ocean Engineering* **2022**, *257*, 111615. https://doi.org/10.1016/j.oceaneng.2022.111615.
22. Cao, X.; Zhou, Z.; Zhang, H.; Zhang, N. A review on the stability of towed floating bodies during wet towing operations. *Ocean Engineering* **2025**, *340*, 122449. https://doi.org/10.1016/j.oceaneng.2025.122449.
23. Shames I.H. *Mecánica de fluidos*, 3rd ed.; Publisher: Faculty of Engineering and Applied Science, New York, USA, 2008; pp. 154–196. https://www.academia.edu/8066544/Mecanica_de_fluidos_shames.
24. Streeter, V.A. *Mecánica de los fluidos*, 1st ed.; Publisher: McGraw-Hill Inter Americana, s. a., 2000; p. 747. https://www.google.cz/books/edition/Mecánica_de_los_fluidos/CMsK0QEACAAJ?hl=cs.
25. Atua, K.; Ayyub, B.M. Reliability analysis of transverse stability of surface ships. *Naval Engineers Journal* **2009**, *109*(3), pp. 129–140. https://doi.org/10.1111/j.1559-3584.1997.tb03175.x.
26. Haddara, M.R.; Wishahy, M.; Wu, X. Assessment of ship's transverse stability at sea. *Ocean engineering* **1994**, *21*(8), pp. 781–800. https://doi.org/10.1016/0029-8018(94)90053-1.
27. Megel, J.; Kliava, J. Metacenter and ship stability. *American Journal of Physics* **2010**, *78*(7), pp. 737–747. https://doi.org/10.1119/1.3285975.
28. Hrabovsky, L. Příčná stabilita plovoucího tělesa válcového tvaru plováků (In English: Transverse stability of a floating body with cylindrical-shaped floats), *Perner's Contacts* **2010**, *5*(1), pp. 85–94. https://pernerscontacts.upce.cz/index.php/perner/article/view/942.
29. Hrabovsky, L. Podélná stabilita plovoucího tělesa válcového tvaru plováků–1. fáze (In English: Longitudinal stability of a floating body with cylindrical-shaped floats – Phase 1.), *Perner's Contacts* **2010**, *5*(3), pp. 84-94. https://pernerscontacts.upce.cz/index.php/perner/article/view/997.
30. Lazecky, P. Stabilita plovoucího dopravníku s koncovými plováky (In English: Stability of floating conveyor with end floats), Bachelor's thesis, VSB–Technical University of Ostrava, 2012. http://hdl.handle.net/10084/93886.
31. Livecka, E.; Melzer, L. *Vodní bagrování* (In English: *Water dredging*), 1st ed.; Publisher: SNTL, Czech Republic, 1964; p. 302. https://vufind.mzk.cz/Record/svkpk.PNA01-000303323.
32. Mathcad 14.0–User's Guide. Available online: https://www.scribd.com/doc/3239532/Mathcad-14-Users-Guide (accessed on 8. May 2007).
33. Pagac, M. *Učebnice SolidWorks* (In English: *SolidWorks textbook*), Vydavatelství Nová media s. r. o.: Prague, Czech Republic, 2020; p. 416, ISBN 978-80-270-0918-3. https://eshop.solidvision.cz/ucebnice-solidworks-2/.
34. PLEXIGLAS® Trubky a tyče Technický list (In English: LEXIGLAS® Tubes and Rods – Technical Data Sheet). Available online: https://www.zenit.cz/public/media/Plasty/Zenit_Technicky_List_Plasty_Plexiglas_trubky_tyce.pdf?_ga=2.46977383.1190389475.1773304708-1782010313.1773304708 (accessed on 13. August 2025).

 doi:10.20944/preprints202604.1700.v1

35. Tenzometrický snímač síly EMS30 (In English: EMS30 Strain Gauge Force Sensor). Available online: https://www.emsyst.sk/products/force-sensors/standard/files/EMS30_sk.pdf (accessed on 28. July 2025).
36. Technical reference manual DS–NET V20–1. Available online: https://d36j349d8rqm96.cloudfront.net/3/6/Dewesoft-DS-NET-Manual-EN.pdf (accessed on 17. November 2016).
37. User manual Getting started with Dewesoft® V21–1 Available online: dewesoftx-getting-started-manual-en.pdf (accessed on 7. January 2021).
38. Madr, V.; Knejzlik, J.; Kopecny, I.; Novotny, I. *Fyzikální Měření* (In English: *Physical Measurement*), SNTL: Prague, Czech Republic, 1991; p. 304, ISBN 80-03-00266-4.
39. Hrabovsky, L.; Maslaric, M. Device designed for detection and setting the required tensile force in ropes. *Advances in Science and Technology. Research Journal* **2018**, *12*(1), pp. 200–206. DOI: 10.12913/22998624/86614.
40. Thompson, J.M.T.; Rainey, R.C.T.; Soliman, M.S. Ship stability criteria based on chaotic transients from incursive fractals. *Philosophical Transactions of the Royal Society of London. Series A: Physical and Engineering Sciences* **1990**, *332*(1624), pp. 149–167. https://doi.org/10.1098/rsta.1990.0106.
41. Surendran, S.; Reddy, J.V.R. Numerical simulation of ship stability for dynamic environment. *Ocean* Engineering **2003**, *30*(10), pp. 1305–1317. https://doi.org/10.1016/S0029-8018(02)00109-9.